Journal of Physics B: Atomic,
Molecular and Optical Physics

3dnl $J=0^e$-2^e autoionizing levels of calcium: observation by laser optogalvanic spectroscopy and theoretical analysis

To cite this article: S Assimopoulos *et al* 1994 *J. Phys. B: At. Mol. Opt. Phys.* **27** 2471

J. Phys. B: At. Mol. Opt. Phys. 27 (1994) 2471–2496. Printed in the UK

3dnl $J = 0^e$–2^e autoionizing levels of calcium: observation by laser optogalvanic spectroscopy and theoretical analysis

S Assimopoulos†, A Bolovinos†, A Jimoyiannis†, P Tsekeris†, E Luc-Koenig‡ and M Aymar‡

† Atomic and Molecular Physics Laboratory, Physics Department, University of Ioannina, GR-451 10 Ioannina, Greece
‡ Laboratoire Aimé Cotton, CNRS II, Bâtiment 505, 91405 Orsay Cedex, France

Received 9 December 1993, in final form 7 April 1994

Abstract. The even parity $J = 0$–2 autoionizing spectra of calcium are investigated below the 3d threshold by a two-step laser excitation from the 3d4s metastables through the 3d4p $^3P_{0,1,2}$ intermediate states. The 3d4s are populated by electronic collisions in a DC glow discharge through a Ca heat-pipe.

Around 300 resonance transitions are measured with an accuracy of ~0.2 cm^{-1} for the narrow ones using standard laser calibration techniques. Their upper levels are assigned to 17 autoionizing 3dns, 3dnd and 3dng Rydberg series and several perturbers belonging to the 4p^2 and 4p5p configurations.

The theoretical interpretation is achieved by a combination of the eigenchannel R-matrix and multichannel quantum defect (MQDT) methods. Five, twelve and fourteen interacting channels are introduced for $J = 0$, $J = 1$ and $J = 2$ series respectively. Theoretical energy level positions and excitation profiles are compared with the experimental data, confirming the identification of the observed structures and pointing out the behaviour of the different perturbed Rydberg series.

1. Introduction

The study of two-electron systems is of particular interest for understanding much of the atoms. The simplest case to treat theoretically is helium, but its high excitation energies are very inconvenient for experimental investigations. Alkaline earths are the next choice and they are actually very appropriate for such studies. Their two external s^2 electrons have excitation energies within the range of easily available light sources and, at the same time, well below the excitation energies of the closed shell electrons of the ionic core.

The availability of tunable dye lasers and the application of multistep and multiphoton excitation schemes have provided a large number of data on the excited atomic states of such atoms with different angular momenta and either parity. Among the atoms investigated up to now experimentally in the autoionization regime, Ba has been the most extensively studied (Camus *et al* 1983, Jones *et al* 1991, Bente and Hogervost 1989a and references therein) followed by work on Sr (Jimoyiannis *et al* 1993 and references therein, Goutis *et al* 1992), while Ca is less explored (Garton and Codling 1965, Brown *et al* 1973, Morita and Suzuki 1988, Morita *et al* 1988).

0953-4075/94/122471+26$19.50

The even parity 5dnl series of Ba and 4dnl series of Sr have been extensively investigated by laser spectroscopy. Series with $J=0$–5 were observed in Ba (Camus *et al* 1983) and Sr (Jimoyiannis *et al* 1992, 1993) using two-step optogalvanic spectroscopy. Two-step laser experiments in an atomic beam allowed the observation of $J=2$–4 series of Ba (Bente and Hogervost 1989b) and $J=0$–2 series of Sr (Kompitsas *et al* 1991, Goutis *et al* 1992). In contrast the homologous even parity 3dnl spectrum of Ca was up to two years ago practically unexplored. A recent theoretical work (Aymar and Telmini 1991) carried out with a combination of the eigen channel R-matrix and multichannel quantum defect (MQDT) methods has been followed by a laser optogalvanic experiment (Bolovinos *et al* 1992). These works dealt only with the $J=0^e$ and $J=2^e$ spectra, data being reported for 3dnl Rydberg levels with $n \leqslant 15$ only. In this report we present additional experimental and theoretical results obtained with the same method for the $J=0^e$ and $J=2^e$ spectra of Ca and new results for the $J=1^e$ spectra.

In the energy range between the first 4s (49 305.95 cm^{-1}), the second $3d_{3/2}$ (62 956.14 cm^{-1}) and third $3d_{5/2}$ (63 016.83 cm^{-1}) ionization limits several 4p5p $J=0$–2 levels as well as the $4p^2\ ^1S_0$ are expected to lie, and we were able to observe most of them. These perturbers affect strongly the quantum defects, transition probabilities and linewidths of the 3dnl Rydberg series. In Sr the analogous 5p6p and 5p^2 perturbers are found in the same autoionization range (Goutis *et al* 1992), while in Ba the $6p^2\ ^1S_0$ only is found there and the 6p7p are above the $5d_{5/2}$ threshold (Camus *et al* 1983).

The Ca levels reported here are detected in a DC glow discharge by a two-step laser optogalvanic (OG) technique. In such a discharge the Ca even parity metastable levels 3d4s, which are ~20 000 cm^{-1} above the ground $4s^2\ ^1S_0$ level, are sufficiently populated by electronic collisions. From these metastables we can excite in the first step the odd-parity 3d4p $^3P_{0,1,2}$ levels using laser light in the green spectral range. In the second step we reach the dipole allowed 3dns and 3dnd $J=0$–3 levels, as well as the 3dng ones in as much as there is configuration mixing on the initial or final levels, using laser light in the blue and green mostly. The $J=3$ levels are going to be looked at through the 3d4p $^1F_3$ intermediate also and will be published separately, while preparations are under way for exciting the 3d4p $^3F_{3,4}$ intermediates, using UV laser light, in order to cover the even-parity 3dnd and 3dng levels up to $J=5$.

The advantage of the above technique, beside its simplicity, is that we can reach high energy and high angular momentum levels using only two easily available laser wavelengths. If we had to start from the ground $J=0$ level, we would need more steps (up to five for $J=5$) to reach the same levels and this would introduce complexity in the experimental set-up and the analysis of the results. In addition, since the excitation cross section for the different 3dnl series depends on the particular intermediate level, the choice of the most convenient one is more easily made from the several 3d4s initial levels that are available. On the other hand the small fluctuating local electric fields of the discharge produce, through the Stark effect, a line broadening and a subsequent peak amplitude reduction of the transitions to the strongly polarizable high n Rydberg levels. This reduces the resolution and detectability of the method to levels not higher than $n \sim 40$. Excitation of the metastables 3d4s in an atomic beam by an electron beam (Bente and Hogervost 1989b) or a hollow cathode discharge (Salih and Lawler 1983) is a good way to extend the resolution and detection limits to higher n members.

The theoretical results presented here are obtained with the jj-coupled R-matrix method rather than the LS-coupled R-matrix, followed by a frame transformation used in the previous paper (Aymar and Telmini 1991). Therefore for the low lying levels

($n \leqslant 15$) of the $J=0^e$ and 2^e spectra, the present results differ slightly from the previous ones; new results for these spectra as well as for the $J=1^e$ are added. The 3dng channels, previously disregarded, have been included. Moreover photoionization spectra from the various intermediates used experimentally have been calculated and have proved to be very useful for the assignment of the J value to an autoionizing level. The calculations have been very helpful in interpreting the irregularities of the energy positions and spectral shapes of the autoionization resonances.

2. Experimental method

The experimental method has been described before (Camus *et al* 1979, Jimoyiannis *et al* 1992). Two-step excitations are induced in a glow discharge through a Ca heat-pipe, which uses He as a buffer gas. A 3 mJ nitrogen laser (SOPRA 804C) is used to pump, at a frequency of 17 Hz, a home-made dye laser oscillator for the first excitation step at wavelength λ_1 and a commercial dye laser oscillator–amplifier (SOPRA LCR I) for the second step at λ_2. Both dye lasers have a linewidth of 0.3–0.4 cm^{-1}. A part of the scanning laser beam λ_2 is sent into a home-made Fabry–Perot interferometer (1.841 ± 0.001 cm^{-1} free spectral range) operating under vacuum. The light intensity interference fringes, which are produced as λ_2 is varied, are detected with a fast photodiode (MRD 500) and are used for wavelength calibration. The two-step OG spectrum of Ca and the Fabry–Perot fringes are processed via two gated integrators (PAR 164/165) and are finally recorded on a dual pen recorder.

The heat-pipe, similar to that of Camus (1974), is a 30 cm long quartz tube of 15 mm diameter with two removable electrodes from stainless steel (anode) and nickel (cathode). The heated region has a length of ~15 cm and includes a thin stainless steel tube with a stainless steel mesh as a wick. The discharge is maintained by a well stabilized HV power supply and the optimum operation conditions are 600–700 V, for total voltage, and 12–18 mA for the ~3.5 Torr of gas pressure which is the Ca vapour pressure at the operating temperature of ~900 °C (Nesmeyanov 1963). The discharge noise level is no more than 5 mV, when seen in an oscilloscope with 1 MΩ input impedance.

When the dye laser light is tuned in resonance with an atomic transition, it strongly perturbs the discharge. The perturbation causes an impedance change and can be measured as a voltage change, called the OG signal, across a ballast resistor. It is taken care, by choosing the laser intensity, that the first excitation step from the 3d4s metastables to the 3d4p $^3P_{0,1,2}$ intermediates produces an OG signal of 10–50 mV, in which case the two-step OG signal attains peak amplitudes up to a few volts for the stronger transitions.

3. Theoretical analysis

The analysis of the experimental data is performed using the eigenchannel R-matrix method in combination with MQDT, i.e. using an approach presented in several papers (Aymar *et al* 1987, Kim and Greene 1987, Greene and Aymar 1991). The same method was previously used to predict the $J=0^e$ and $J=2^e$ spectra of Ca (Aymar and Telmini 1991) and to interpret the $J=0^e$ (Kompitsas *et al* 1991) and $J=1$–2^e (Goutis *et al* 1992) spectra of Sr in the autoionizing energy range below the 4d$_{5/2}$ threshold, homologous to that studied in Ca in the present work. Readers should refer to the above papers for details on the computation. Here only some points are outlined.

The calculations are performed in *jj*-coupling with the spin–orbit interaction included explicitly with the *R*-matrix reaction volume. The *jj*-coupled *R*-matrix approach is chosen rather than the *LS*-coupled *R*-matrix method followed by a (*jj*–*LS*) frame transformation as used previously (Aymar and Telmini 1991). Indeed this accounts for intermediate coupling effects in the initial 3d4p levels and results in a better description of the photoionization spectra (Telmini *et al* 1993). Some other differences with the previous work (Aymar and Telmini 1991) should be noted. A larger *R*-matrix box of radius $r_0 = 25$ au instead of 15 au improves the description of the initial 3d4p ^{3}P levels and that of the 4d*n*g levels which are now included in the calculations. In fact the larger r_0 value incorporates some long range non-Coulomb effects, neglected previously, whose role is important for g-levels. A last difference concerns the model potential used to describe the Ca^{2+}–e interaction, whose quality determines the accuracy of the final results. This *l*-dependent model potential is presently adjusted to reproduce the $Ca^+(nlj)$ energy levels, contrary to the potential used in the *LS*-coupled *R*-matrix calculations which was optimized on the $Ca^+(nl)$ spin-average levels. The $l = 2$ orbitals are difficult to describe because the $3d_j$ fine structure splitting in Ca^+ is very sensitive to two effects with opposite contribution; on the one hand the collapse of the d orbital (Griffin *et al* 1969) results in a contraction to smaller radii and therefore in an increase of the splitting, while on the other the anomalous fine structure effects (Sternheimer 1979), observed in several excited levels ($l \geqslant 2$) in alkali like spectra, and especially in, the isoelectronic with Ca^+, pottasium, corresponds to fine structure splittings very much smaller, even inverted, than predicted by a single electron non-relativistic model (Foley and Sternheimer 1975, Luc-Koenig 1976).

Two types of calculations are performed. The first one concerns the determination of the energy positions and wavefunction compositions of doubly excited $J = 0^e$–2^e levels using effective reaction matrices restricted to closed channels only, as described elsewhere (Aymar and Telmini 1991). New energy values obtained for $J = 0^e$ and $J = 2^e$ levels agree well with those previously published (Aymar and Telmini 1991). The second type of calculation deals with the partial photoionization cross sections $\sigma(E)$ (in Mb) for the various 3d4p $^3P^o_J \rightarrow J$ excitation processes with unpolarized light; the energy dependence of $\sigma(E)$, calculated on a given energy mesh, presents resonance structure whose FWHM gives the autoionization width of the doubly excited states. The resonant peak positions agree, within the autionization widths, with the energy positions deduced from the effective reaction matrices.

Calculations for $J = 0^e$, 1^e and 2^e involve five, twelve and fourteen interacting channels, homologous to those used in Sr (a complete list can be found for $J = 0^e$ in table 2 of Aymar and Telmini (1991) and for $J = 1^e$, 2^e in table 1 of Goutis *et al* (1992)).

4. Experimental results

Figure 1 shows the OG signals produced by exciting a typical autoionizing region through the different 3d4p ^3P_J intermediate levels. Applying the $\Delta J = 0, \pm 1$ ($J = 0 \leftarrow / \rightarrow J = 0$) selection rules, the J values of the 3d*nl* states can be easily derived in principle. Those reached from $^3P_0$ have $J = 1$, while through $^3P_1$ and $^3P_2$ we can reach states with $J = 0, 1, 2$ and $J = 1, 2, 3$ respectively. Thus we can deduce the J value of the different autoionizing states by looking through which intermediates they are observed. Nevertheless, since their transition strength depends also on the particular intermediate used, some transitions may be so weak that we cannot see them. In addition some lines

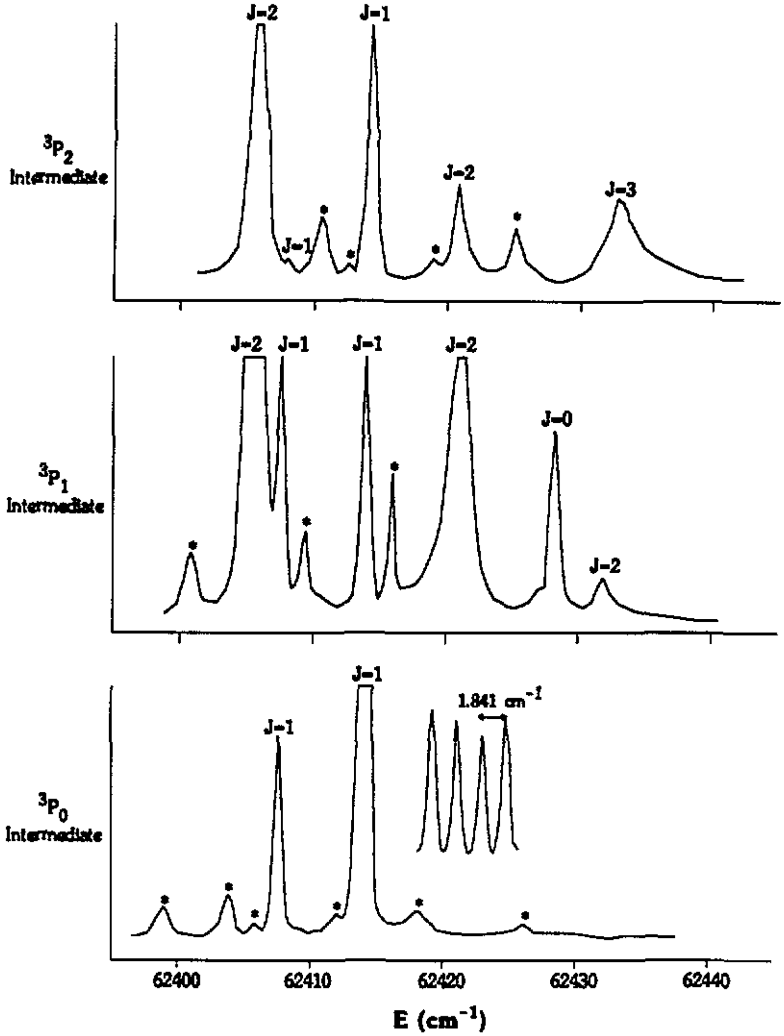

Figure 1. Two-step OG spectrum of Ca through the 3d4p $^3P_{0,1,2}$ intermediates. 'False' transitions (see text) are shown with asterisks (*). A part of laser λ_2 light interference fringes pattern is also included.

are hidden under much stronger ones, which are usually due to transitions between bound Ca states. For example, in the figure 1 we can see that the transition to the $J=1$ level at 62 407.7 cm^{-1} is barely seen through the $^3P_2$ intermediate and the transition to the $J=2$ level at 62 432.2 cm^{-1} is seen clearly only through the $^3P_1$ intermediate while in the spectrum through the $^3P_2$ intermediate it is covered by a broader transition to a $J=3$ state. Thus the non-detecting of some lines may guide us to erroneous assignments, if we use the J selection rules solely. Theoretical predictions on energy positions, line intensities and linewidths, as well as experimental trends concerning the widths and intensities of the different observed series, proved to be decisive for a correct assignment in many cases.

We detect also transitions from the other intermediate levels of the same multiplicity as the intermediate state we are exciting in the first step. For example, when we excite the 3d4p $^3P_1$ intermediate, we see transitions in the second step that start from the 3d4p $^3P_0$ and 3d4p $^3P_2$ levels too. These $^3P_0$ and $^3P_2$ levels are populated through collisions in the discharge environment, since their energy differences from the laser-excited level $^3P_1$ are small enough for such a population mechanism to be sufficiently effective. These 'false' transitions, which are indicated with asterisks in figure 1, can easily be singled out. They occur at the same λ_2, irrespectively of the excited 3d4p ^3P_J in the first step, and they have at least an order of magnitude lower intensity than the real ones which appear when the corresponding intermediate is excited directly by the first laser and not through collisions.

The spectral lines that are due to known transitions between bound Ca levels are used as internal calibration standards for the experimental determination of the energies of the 3d4p→3dnl transitions. The accuracy of our results is estimated to be $\leqslant \pm 0.2$ cm^{-1} for sharp lines, 2 or 3 times worse for the broader and/or weaker lines and ~1 cm^{-1} for a couple of very broad ones. Using different discharge conditions we found no change (which might be due to Stark shifts) in the spectral positions within these accuracy limits. This agrees with the low electric field strength in the possitive column (a few V cm^{-1}), and is in agreement with similar work on Ba (Camus *et al* 1982) and Sr (Jimoyiannis *et al* 1992).

Since the two 3d ionization thresholds are very close ($\Delta E_{3d} \sim 60$ cm^{-1}), in contrast to the cases of Sr ($\Delta E_{4d} \sim 280$ cm^{-1}) and Ba ($\Delta E_{5d} \sim 800$ cm^{-1}), the detectivity of our method ($n \leqslant 40$) limits us to the region below the $3d_{3/2}$ threshold. The ~300 levels we detected cover the energy range from ~57 600 cm^{-1} to ~62 900 cm^{-1}. The 4pnp levels that perturb the 3dnl $J=0$–2 spectra are the '4p^2' $^1S_0$ and 4p5p $^3P_0$, the 4p5p $^1P_1$, $^3D_1$ and the 4p5p $^3D_2$ and $^3P_2$.

In table 1 we give the experimental and theoretical energies of the observed 3dnd $J=0$ autoionizing levels and of a perturber belonging to the 4p^2 configuration (the energies are with reference to the 4s^2 $^1S_0$ ground level), their effective quantum numbers relative to the $3d_{3/2}$ and $3d_{5/2}$ ionization thresholds, the *jj*-coupled levels that are calculated to contribute significantly to each particular wavefunction (if two or more *jj*-levels have a contribution of more than 10%, we give the two with the highest percentage), the relative peak intensity of the observed transition through the 3d4p $^3P_1$ intermediate and the experimental linewidths. The reported linewidths have a lowest limit of ~0.3 cm^{-1} at low n values that is due to the laser bandwidth, while at high n states, which are more sensitive to Stark and collision broadening, the experimental limit is $\geqslant 1$ cm^{-1}. Tables 2 and 3 give the corresponding results for the $J=1$ and $J=2$ levels; the intermediate levels through which they are excited are the 3d4p $^3P_0$, $^3P_1$, $^3P_2$ and 3d4p $^3P_1$, $^3P_2$ respectively.

A rapid examination of these tables shows a perfect agreement between theoretical and experimental energies for excited levels (less than 1 cm^{-1} in the vast majority of cases). The less satisfactory concordance observed for the low lying levels arises from the difficulties encountered by the R-matrix method in studying the lowest members of the Rydberg series (Greene and Aymar 1991) and by the description of the d orbitals.

From the results given in tables 1–3, we can notice some general trends that characterize the different 3dnl series. We can discern a group of narrow and weak lines, seen up to $n \sim 15$, which correspond to levels with a quantum defect of $\leqslant 0.02$. They are due to the electric dipole forbidden 3d4p→3dng transitions. The high $l=4$ value of the external ng electron implies that its core penetration is very small and this can explain both their near-zero quantum defect and the small autoionization width.

The second group of transitions with linewidths of 1–15 cm^{-1} and weak peak intensities populates levels with quantum defects of ~2.3. It is ascribed to the 3d4p→3dns

Table 1. Energies, linewidths, relative transition intensities via the indicated intermediate levels and effective quantum numbers relative to the $3d_{3/2}$ and $3d_{5/2}$ ionization limits for observed $J=0^e$ Ca autoionizing levels. The last two columns give the theoretical energies, obtained from the resonant peaks of the calculated $\sigma(E)$ spectrum, and the assignment to *jj*-coupled levels of the 3d*n*d, 3d*n*s or 3d*n*g configurations. The perturber level of the $4p^2$ configuration is identified in the *LS* coupling scheme. The largest weights in the wavefunction expansion are indicated in brackets. The E_{theor} values correspond to the maxima of the cross sections $\sigma(E)$. R, overlap with a stronger transition due to a close-lying $J\neq 0$ Rydberg state. *, the energy value is that of the overlapping stronger Rydberg state. sh, transition appears as a shoulder to a near-lying one. Peak amplitude estimates: vvs (very very strong), vs (very strong), s (strong), m (medium), w (weak), vw (very weak). *n*d−− and *n*d++ stand for $3d_{3/2}nd_{3/2}$ and $3d_{5/2}nd_{5/2}$ respectively. The numbers in brackets give the percentage contribution to the wavefunction of the corresponding mainly involved configurations (for the $4p^2$ the respective number gives the total contribution of this configuration).

E_{exp} (cm^{-1})	Width (cm^{-1})	$^3P_1$	$^1P_1$	$\nu^*_{3/2}$	$\nu^*_{5/2}$	E_{theor} (cm^{-1})	Assignment
57 611.1	0.9	vs		4.531	4.506	57 691.4	5d−−, 5d++ [57, 42]
58 535	~90		w	4.982	4.948	58 762	$4p^2\ ^1S_0$5d++, 5d−− [35, 39, 26]
59 351.6	0.4	s		5.518	5.472	59 385.8	6d−−, 6d++ [66, 33]
59 594.0	3.5		s	5.713	5.662	59 702.7	6d++, 6d−−$4p^2$ [62, 27, 11]
60 361.4	0.5	vvs		6.503	6.428	60 377.3	7d−−, 7d++ [79, 20]
60 481.6	0.5	s		6.659	6.579	60 518.8	7d++, 7d−− [79, 19]
60 998.6	0.7	vs		7.487	7.374	61 006.4	8d−−, 8d++ [86, 12]
61 090.3	0.9	w		7.669	7.547	61 107.9	8d++, 8d−− [87, 12]
61 426.7	0.7	vs		8.470	8.307	61 430.6	9d−−, 9d++ [89, 9]
61 508.0	0.6	s		8.705	8.528	61 517.9	9d++, 9d−− [90, 10]
61 728.2	0.6	s		9.453	9.228	61 730.2	10d−−, 10d++ [90, 8]
61 804.3	1.0	m		9.761	8.513	61 810.1	10d++, 10d−− [91, 9]
61 948.5	0.9	vs		10.436	10.135	61 949.8	11d−−, 11d++ [91, 7]
62 020.8	0.8	s		10.832	10.496	62 024.7	11d++, 11d−− [91, 9]
62 114.5	0.6	vs		11.419	11.028	62 115.6	12d−−, 12d++ [90, 8]
62 183.7	0.8	s		11.919	11.477	62 186.2	12d++, 12d−− [88, 11]
62 242.9	0.8	s		12.404	11.908	62 244.3	13d−−, 12d++ [88, 10]
62 308.7	0.8	s		13.019	12.449	62 310.4	13d++, 14d−− [82, 17]
62 345.0	0.8	s		13.400	12.780	62 346.6	14d−−, 13d++ [83, 16]
62 405.4*	—	R		14.116	13.397	62 407.0	14d++, 15d−− [67, 31]
62 428.5	0.8	m		14.421	13.657	62 430.1	15d−−, 14d++ [69, 31]
62 480.8	0.6	s		15.194	14.308	62 481.9	16d−−, 15d++ [55, 42]
62 498.8	0.7	vw		15.490	14.554	62 500.6	15d++, 16d−− [54, 46]
62 539.7	0.7	vs		16.233	15.165	62 540.8	17d−−, 16d++ [73, 24]
62 559.2	0.8	w		16.627	15.485	62 560.8	16d++, 17d−− [70, 30]
62 587.3	0.8	s		17.249	15.984	62 588.8	18d−−, 17d++ [79, 19]
62 609.8	0.8	m		17.800	16.420	62 611.4	17d++, 18d−− [70, 29]
62 627.8	0.6	m		18.282	16.795	62 629.5	19d−−, 17d++ [76, 23]
62 651.1	0.6	m		18.967	17.322	62 652.6	18d++, 20d−− [54, 44]
62 663.9	0.6	w		19.378	17.633	62 664.9	20d−−, 18d++ [60, 40]
62 686.3*	—	R		20.166	18.221	62 685.6	21d−−, 19d++ [67, 31]
—	—	—				62 697.3	19d++, 21d−− [60, 40]
62 711.8	—	sh		21.192	18.967	62 712.4	22d−−, 19d++ [76, 23]
62 725.4	1.2	m		21.808	19.405	62 726.0	20d++, 22d−− [61, 38]
62 734.9	1.1	s		22.271	19.729	62 735.8	23d−−, 20d++ [76, 23]
62 748.5	1.1	m		22.989	20.223	62 749.4	24d−−, 21d++ [63, 36]
62 756.0	1.0	vw		23.416	20.511	62 757.6	21d++, 24d−− [56, 44]
62 767.5	1.1	s		24.119	20.979	62 768.2	25d−−, 22d++ [76, 23]
62 777.3	1.0	m		24.771	21.404	62 777.8	22d++, 25d−− [54, 46]

Table 1. (continued)

E_{exp} (cm^{-1})	Width (cm^{-1})	$^3P_1$	$^1P_1$	$\nu^*_{3/2}$	$\nu^*_{5/2}$	E_{theor} (cm^{-1})	Assignment
62 784.1	1.1	s		25.256	21.714	62 784.8	26d−−, 22d++ [67, 33]
62 793.0*	—	R		25.935	22.142	62 794.3	27d−−, 23d++ [70, 30]
62 799.6	1.0	vw		26.477	22.476	62 800.8	23d++, 27d−− [54, 46]
62 807.5	1.5	s		27.171	22.896	62 807.7	28d−−, 23d++ [75, 25]
62 814.9	—	sh		27.874	23.312	62 815.2	29d−−, 24d++ [61, 39]
62 819.6	1.3	vw		28.349	23.588	62 820.3	24d++, 29d−− [45, 55]
62 826.9	1.5	m		29.139	24.037	62 826.6	30d−−, 25d++ [77, 22]
62 832.6	1.0	m		29.804	24.406	62 832.6	25d++, 30d−− [44, 55]
62 836.9	1.5	m		30.336	24.696	62 836.9	31d−−, 25d++ [62, 38]
62 842.7*	—	R		31.102	25.104	62 842.4	32d−−, 26d++ [77, 22]
62 847.0	1.0	w		31.709	25.419	62 847.3	26d++, 32d−− [45, 55]
62 850.9	1.5	m		32.291	25.716	62 850.9	33d−−, 26d++ [65, 34]
62 855.3	1.3	m		32.988	26.064	62 855.6	34d−−, 27d++ [78, 21]
62 859.9	1.0	w		33.767	26.444	62 859.8	27d++, 34d−− [42, 58]
62 863.0	1.5	w		34.325	26.709	62 862.9	35d−−, 27d++ [65, 35]
62 867.1*	—	R		35.106	27.072	62 866.9	36d−−, 28d++ [80, 20]
62 870.4	1.0	w		35.775	27.375	62 870.5	37d−−, 28d++ [65, 35]
62 873.4	1.5	w		36.418	27.660	62 873.2	28d++, 37d−− [40, 60]
62 876.5	1.5	w		37.120	27.964	62 876.4	38d−−, 28d++ [80, 19]
62 879.8	1.5	vw		37.914	28.299	62 879.7	39d−−, 29d++ [74, 25]

transitions. The low $l=0$ value of the external electron explains both their large autoionization width and the large quantum defect, because the penetrating $l=0$ orbit interacts strongly with the Ca^+ ion core.

The last and most numerous group consists of transitions to the 3d*n*d levels. The observed lines are stronger in general than those of the previous two groups and have various, but narrow in general, linewidths, larger than the 3d*n*g levels and smaller than the 3d*n*s ones. The quantum defects show variations, with values within the range of 0.4–0.9, indicating that the corresponding levels are much more affected by the perturbations.

5. Analysis of the experimental results

A way to compare experimental and theoretical energy levels is to draw Lu–Fano plots. Such graphs are presented in figures 2–4 where $\nu_{3d_{3/2}}$ (mod 1) and $\nu_{3d_{5/2}}$ are the effective quantum numbers relative to the $3d_{3/2}$ and $3d_{5/2}$ ionization thresholds. In these plots the curves correspond to calculations, the full circles to the theoretical energy levels and the open squares to the observed ones. The observed levels with maximum 4p*n*p character are shown by open triangles.

From the calculated admixture coefficients Z_i (Lee and Lu 1973) of each *jj*-coupled channel *i* we get quantitative information on the wavefunction composition of each level. Because of the interchannel couplings and the mixing of 3d*nl* levels with the $4p^2$ and 4p5p perturbers, for a lot of levels several $|Z_i|^2$ have a non-negligible value. Obviously in such cases the levels are not well described within the *jj* coupling scheme. The weight allowing us to label the levels is given in the last column of tables 1–3.

In the following we present the results concerning the 4p5p perturbers and the various 3d*nl* Rydberg series.

Table 2. Same as table 1 for $J=1^e$ Ca levels. R, sh, *, etc as in table 1. B, overlap with a stronger transition between bound Ca or He states. nd−+, nd+−, ng−−, ns−, etc stand for $3d_{3/2}nd_{5/2}$, $3d_{5/2}nd_{3/2}$, $3d_{3/2}ng_{3/2}$, $3d_{3/2}ns_{1/2}$ etc respectively. In the level assignment we give the contributions above ~10%. At higher n members two close-lying theoretical states are given for one observed level. The preference of one of the two is based on calculated transition intensity trends.

E_{exp} (cm^{-1})	Width (cm^{-1})	$^2P_0$	$^3P_1$	$^3P_2$	$\nu^*_{3/2}$	$\nu^*_{5/2}$	E_{theor} (cm^{-1})	Assignment
58 620.3	0.25	s	R	R	5.031	4.996	58 620.3	5g+− [100]
58 761.4	2.0	vvs	vs	—	5.115	5.078	58 757.6	6d−− [97]
58 807.9	1.2	vvs	m	s	5.143	5.106	58 801.5	6d−+, 6d+− [41, 38]
58 843.8	1.5	s	vvs	vs	5.166	5.128	58 835.6	6d++ [81]
59 363.5	0.25	vs	R	R	5.527	5.481	59 396.7	6d+−, 6d−+ [51, 48]
59 960.4	0.25	m	R	R	6.052	5.992	59 958.9	6g+− [100]
60 022.6	1.6	m	s	B	6.116	6.054	60 020.0	7d−− [99]
60 062.6	1.2	vs	m	vs	6.158	6.095	60 059.2	7d−+, 7d+− [48, 40]
60 094.3	0.9	m	vvs	vvs	6.192	6.128	60 089.7	7d++ [88]
60 379.1	0.4	vvs	vvs	vvs	6.525	6.450	60 393.8	7d+−, 7d−+ [54, 45]
60 770.3	0.5	w	R	R	7.085	6.989	60 768.8	7g+− [100]
60 779.6	1.3	—	w	—	7.101	7.004	60 777.9	8d−− [91]
60 820.4	1.1	m	w	m	7.168	7.068	60 819.0	8d−+, 8d+− [49, 35]
60 850.3	0.9	w	s	vs	7.219	7.117	60 847.6	8d++ [80]
61 021.0	0.5	s	vs	vs	7.530	7.415	61 027.2	8d+−, 8d−+ [57, 41]
61 132.1	1.7	w	m	—	7.756	7.630	61 146.6	**4p5p ^{1}P$_1$** [72]
61 296.6	0.5	vw	R	R	8.132	7.987	61 295.1	8g+− [97]
61 300.0	1.0	vw	—	—	8.140	7.995	61 301.0	9d−−, 9d−+ [67, 12]
61 328.2	1.0	w	vs	m	8.210	8.061	61 328.0	9d−+, 9d+− [50, 27]
61 375.0	1.0	w	vw	m	8.331	8.175	61 377.8	9d++, 4p5p [78, 13]
61 452.6	0.4	s	vs	vvs	8.543	8.376	61 455.2	9d+−, 9d−+ [63, 35]
61 501.3	3.5	w	w	—	8.685	8.509	61 506.8	11s− [97]
61 622.5	10	w	vw	—	9.071	8.871	61 627.0	10d−−, 4p5p [64, 16]
61 656.6	0.8	m	m	R	9.189	8.982	61 655.8	9g+− [86]
61 661.5	1.3	—	m	R	9.207	8.998	61 661.4	10d−+, 10d+− [50, 20]
61 693.8	4.6	s	w	R	9.324	9.107	61 697.7	10d++, 4p5p [72, 13]
61 728.9	6.5	vs	m	—	9.456	9.231	61 740.4	**4p5p ^{3}D$_1$**, 10d++ [46, 23]
61 758.3	0.45	s	s	vvs	9.571	9.338	61 758.8	10d+−, 10d−+ [72, 24]
61 802.0	15.0	s	R	—	9.751	9.504	61 805.4	12s−, 4p5p [83, 19]
61 892.9	0.8	vs	vs	—	10.159	9.881	61 893.2	11d−− [96]
61 910.7	0.7	vvs	—	—	10.245	9.960	61 910.7	11d−+, 10d+− [73, 18]
61 916.7	0.7	m	R	R	10.275	9.987	61 916.2	10g+− [94]
61 953.0	0.7	vs	vs	—	10.459	10.156	61 953.0	11d++ [98]
61 982.2	0.8	vs	vs	vvs	10.615	10.299	61 982.1	11d+−, 11d−+ [79, 19]
62 001.7	8.4	m	m	—	10.723	10.397	62 003.4	13s− [198]
62 073.5	0.5	vs	vs	—	11.150	10.786	62 073.5	12d−− [99]
62 088.6	0.6	vvs	s	m	11.247	10.873	62 088.6	12d−+, 11d+− [85, 13]
62 134.4	0.6	m	s	—	11.556	11.152	62 134.2	12d++ [99]
62 151.8	0.7	vs	vs	vvs	11.680	11.263	62 151.8	12d+−, 12d−+ [84, 14]
62 156.0	7.5	m	m	—	11.711	11.291	62 158.4	14s− [99]
62 212.4	0.6	vs	vs	—	12.147	11.680	62 212.4	13d−− [100]
62 224.3	0.6	vvs	s	s	12.245	11.767	62 224.4	13d−+ [89]
62 273.3	0.6	m	m	vw	12.677	12.149	62 273.1	13d++ [98]
62 277.8	6.0	w	w	—	12.719	12.185	62 278.4	15s− [98]
62 283.8	0.6	s	s	vs	12.776	12.235	62 283.6	13d+−, 13d−+ [88, 10]
62 321.1	0.7	vs	s	—	13.145	12.559	62 321.1	14d−− [100]
62 329.9	0.6	vvs	s	vs	13.237	12.639	62 330.2	14d−+ [91]
62 372.3	2.5	w	w	—	13.710	13.048	62 373.4	16s− [100]
62 382.2	0.6	m	m	—	13.827	13.150	62 381.8	14d++ [99]

Table 2. (continued)

E_{exp} (cm^{-1})	Width (cm^{-1})	$^2P_0$	$^3P_1$	$^3P_2$	$\nu^*_{3/2}$	$\nu^*_{5/2}$	E_{theor} (cm^{-1})	Assignment
62 387.9	0.6	m	s	vs	13.897	13.209	62 387.8	14d+−, 14d−+ [89, 10]
62 407.7	0.7	m	m	vw	14.145	13.422	62 407.6	15d−− [100]
62 414.3	0.6	vs	s	s	14.231	13.495	62 414.7	15d−+ [90]
62 449.0	2.5	w	w	—	14.710	13.902	62 449.8	17s− [100]
62 455.4	0.6	vw	vw	—	14.804	13.981	62 455.5	14g+− [100]
62 468.4	0.5	w	m	—	15.000	14.145	62 468.4	15d++ [99]
62 471.1	0.6	—	m	R	15.041	14.180	62 471.2	15d+−, 16d−+ [80, 19]
62 477.6	0.5	m	m	—	15.143	14.266	62 477.7	16d−− [100]
62 483.1*	—	B	B	R	15.231	14.339	62 483.6	16d−+, 15d+− [80, 17]
62 511.6	2.2	w	w	—	15.712	14.738	62 512.2	18s− [100]
62 528.0	0.6	vw	vw	—	16.010	14.983	62 528.0	15g+− [100]
62 535.0	0.5	sh	m	w	16.142	15.091	62 535.0	17d−− [99]
62 535.8	0.6	m	—	—	16.157	15.104	62 535.9	17d−+, 16d+− [74, 24]
62 538.5	0.7	m	—	—	16.210	15.146	62 538.4	16d++ [97]
62 542.8	0.6	B	B	s	16.294	15.215	62 543.2	16d+−, 17d−+ [73, 25]
62 563.2	2.0	w	w	—	16.711	15.553	62 563.6	19s− [100]
62 582.8	0.7	—	m	—	17.144	15.901	62 582.7	18d−− [100]
62 583.5	0.7	vs	w	m	17.160	15.913	62 584.2	18d−+ [96]
62 595.7	1.0	vw	—	—	17.448	16.142	62 595.8	17d++ [99]
62 597.2	0.5	s	m	s	17.485	16.171	62 598.0	17d+− [95]
62 606.0	1.6	w	w	—	17.703	16.343	62 606.7	20s− [100]
62 622.8	0.6	s	m	—	18.144	16.688	62 622.8	19d−− [100]
62 623.5	0.7	—	—	m	18.163	16.703	62 623.8	19d−+ [98]
62 642.3	—	sh	—	—	18.699	17.117	62 642.8	21s− [93]
—	—	—	—	—			62 643.6	18d++ [93]
62 643.8	0.6	m	m	m	18744	17.152	62 644.6	18d+− [97]
—	—	—	—	—			62 656.6	20d−− [100]
62 656.6	0.5	vs	w	m	19.137	17.451	62 657.4	20d−+ [98]
							62 683.5	19d++ [97]
62 683.4	0.7	s	m	s	20.059	18.141	62 684.0	19d+−, 21d−+ [89, 10]
—	—	—	—	—			62 685.6	21d−− [100]
62 685.4	0.6	vs	R	R	20.133	18.196	62 686.4	21d−+ [88]
62 700.2	1.0	w	w	—	20.706	18.617	62 700.6	23s− [100]
							62 710.6	22d−− [99]
62 710.3	0.7	B	B	m	21.127	18.921	62 710.8	22d−+ [98]
							62 717.4	20d++ [96]
62 716.8	0.6	m	m	B	21.412	19.125	62 717.7	20d+− [95]
62 723.4	1.0	vw	sh	—	21.714	19.338	62 723.6	24s− [100]
							62 732.3	23d−−, 23d−+ [82, 18]
62 731.8	0.7	vs	vw	m	22.117	19.621	62 732.4	23d−+, 23d−− [81, 18]
62 743.3	0.8	w	—	—	22.706	20.030	62 743.6	25s− [100]
							63 746.3	21d++, 21d+− [81, 19]
62 745.7	0.6	s	m	R	22.835	20.118	62 746.4	21d+−, 21d++ [83, 16]
62 750.7	0.7	vs	R	m	23.112	20.306	62 751.2	24d−+ [98]
							62 751.3	24d−− [99]
62 761.3	1.5	w	R	—	23.732	20.723	62 761.1	26s− [100]
62 767.5	0.7	s	R	m	24.119	20.979	62 767.7	25d−+ [96]
62 767.9	—	sh	R	—	24.145	20.996	62 767.9	25d−− [97]
62 770.8	0.9	w	m	s	24.333	21.119	62 771.2	22d+− [91]
62 771.3	0.9	w	R	R	24.366	21.141	62 771.4	22d++ [92]
62 776.5	0.9	w	—	—	24.716	21.368	62 776.6	27s− [100]
62 781.9	0.7	s	sh	m	25.096	21.612	62 782.3	26d−+ [99]
							62 782.5	26d−− [100]

Table 2. (continued)

E_{exp} (cm^{-1})	Width (cm^{-1})	$^2P_0$	$^3P_1$	$^3P_2$	$\nu^*_{3/2}$	$\nu^*_{5/2}$	E_{theor} (cm^{-1})	Assignment
62 790.1	1.3	w	R	—	25.708	22.000	62 790.3	28s− [100]
62 792.4	0.8	m	m	s	25.888	22.112	62 792.8	23d+− [95]
62 792.9	0.8	w	R	R	25.928	22.137	62 793.0	23d++ [96]
62 795.0	0.8	m	R	w	26.096	22.241	62 795.4	27d−+ [99]
							62 795.6	27d−− [100]
62 802.2	1.3	w	w	—	26.699	22.611	62 802.4	29s− [100]
62 806.5	0.7	m	R	w	27.080	22.841	62 806.9	28d−+ [99]
62 807.6	0.6	w	R	—	27.180	22.901	62 807.2	28d−− [100]
62 811.2	0.7	w	w	w	27.516	23.101	62 811.6	24d+− [98]
							62 811.9	24d++ [99]
62 813.3	1.0	vw	—	—	27.717	23.220	62 813.3	30s− [100]
62 817.0	0.7	m	—	vw	28.083	23.434	62 817.3	29d−+ [99]
							62 817.6	29d−− [100]
62 823.0	0.8	vw	R	—	28.709	23.794	62 823.1	31s− [100]
62 826.2	0.7	w	m	w	29.060	23.993	62 826.6	30d−+ [97]
62 826.9	—	sh	R	—	29.139	24.037	62 826.9	30d−− [99]
62 828.2	1.2	w	sh	R	29.287	24.120	62 828.3	25d+− [98]
							62 828.6	25d++ [99]
62 831.9	0.7	vw	R	—	29.720	24.360	62 831.9	32s− [100]
62 834.8	0.8	w	R	vw	30.073	24.553	62 835.1	31d−+ [99]
62 835.5	—	sh	R	R	30.160	24.600	62 835.4	31d−− [100]
62 840.0	1.6	vw	—	—	30.739	24.911	62 839.9	33s− [100]
62 842.2	0.7	m	sh	m	31.034	25.068	62 842.6	32d−+, 26d+− [65, 31]
62 843.2	1.2	w	R	R	31.171	25.140	62 842.9	32d−−[95]
							62 843.0	26d+−, 32d−+ [67, 28]
							62 843.3	26d++ [89]
62 847.1	1.2	vw	R	—	31.724	25.427	62 847.1	34s− [100]
62 849.5	1.2	w	R	R	32.078	25.609	62 849.7	33d−+ [99]
62 850.1	—	sh	R	—	32.169	25.655	62 849.9	33d−−[100]
62 853.7	—	sh	—	—	32.730	25.936	62 853.6	35s− [100]
62 855.3	0.8	w	R	m	32.988	26.064	62 855.7	27d+−, 33d−+ [56, 41]
							62 856.1	27d+−, 34d−+ [36, 33]
62 856.0	0.9	w	R	R	33.103	26.121	62 856.2	34d−−, 34d−+ [71, 16]
62 859.7	1.3	vw	—	—	33.732	26.427	62 859.7	36s− [100]
62 861.7	1.3	vw	—	—	34.088	26.597	62 861.7	35d−+ [99]
							62 862.0	35d−− [100]
62 866.7	0.9	vw	—	—	35.027	27.036	62 867.0	36d−+, 28d+− [85, 14]
							62 867.3	36d−− [99]
							62 867.6	28d+−, 36d−+ [86, 14]
62 868.0	0.8	vw	—	—	35.285	27.154	62 867.9	28d++ [98]
							62 871.9	37d−+ [99]
62 871.7	1.0	vw	—	—	36.050	27.498	62 872.1	37d−− [99]
							62 876.4	38d−+ [97]
62 876.2	1.2	vw	—	—	37.050	27.934	62 876.6	38d−− [96]
							62 880.5	39d−+ [99]
62 880.3	1.3	vw	—	—	38.039	28.350	62 880.7	39d−− [100]

5.1. 4p5p levels

These levels which are low-lying members of the 4p*n*p series, are well described in the *LS* coupling scheme. They perturb mainly the 3d*n*d and 3d*n*s levels. In tables 1–3 we give the 4p*n*p character of the different levels, when its contribution is more than 10%.

Table 3. Same as tables 1 and 2 for $J=2^e$ Ca levels. R, B, sh, *, etc as in tables 1 and 2. The E_{theor} values indicated by O are calculated from effective reaction matrices restricted to closed channels.

E_{exp} (cm^{-1})	Width (cm^{-1})	$^3P_1$	$^3P_2$	$\nu^*_{3/2}$	$\nu^*_{5/2}$	E_{theor} (cm^{-1})	Assignment
						56 460.1^{O}	5d−+, 5d+− [44, 42]
57 578.9	0.9	m	vs	4.517	4.492	57 678.2	5d+−, 5d−+ [35, 34]
57 638.4	0.5	vs	vs	4.543	4.517	57 723.4	5d++ [85]
58 554.3	0.25	m	s	4.993	4.959	58 555.5	5g−− [99]
58 612.4	0.25	m	s	5.026	4.991	58 614.0	5g+−, 5g++ [89, 11]
58 620.3	0.25	s	m	5.031	4.996	58 620.4	5g++, 5g+− [90, 10]
58 787.4	2.8	vvs	m	5.131	5.094	58 785.2	6d−+, 6d+− [52, 48]
59 352.6	0.7	m	m	5.518	5.472	59 353.6	6d−− [94]
59 363.5	0.25	vs	s	5.527	5.481	59 396.7	6d+−, 6d−+ [49, 46]
59 389.4	0.4	s	s	5.547	5.500	59 431.6	6d++ [99]
59 897.4	0.25	m	R	5.990	5.931	59 896.4	6g−− [100]
59 956.7	0.25	w	R	6.049	5.988	59 956.0	6g+−, 6g++ [90, 10]
59 960.6	0.25	s	m	6.053	5.992	59 959.0	6g++, 6g+− [90, 10]
60 051.6	1.8	vs	m	6.147	6.083	60 050.7	7d−+, 7d+− [54, 46]
60 340.0	0.7	m	s	6.477	6.403	60 373.2	7d−− [99]
60 378.0	1.2	vs	vs	6.524	6.449	60 399.8	7d+−, 7d−+ [51, 45]
60 410.0	1.3	vs	vvs	6.565	6.488	60 434.7	7d++ [97]
60 708.7	0.5	w	R	6.988	6.895	60 707.2	7g−− [100]
60 768.3	0.5	w	R	7.082	6.986	60 767.6	7g+− [92]
60 770.3	0.5	m	w	7.085	6.989	60 768.9	7g++ [92]
60 816.7	2.2	m	—	7.162	7.062	60 816.6	8d−+, 8d+− [57, 43]
60 992.1	1.5	w	w	7.475	7.362	61 012.8	8d−− [97]
61 023.7	1.0	s	vs	7.536	7.420	61 035.8	8d+−, 8d−+ [51, 40]
61 054.3	1.5	m	s	7.596	7.478	61 070.1	8d++ [94]
61 235.1	0.5	m	R	7.985	7.848	61 234.4	8g−− [100]
61 295.3	0.4	m	R	8.128	7.984	61 294.8	8g+− [98]
61 296.6	0.5	m	w	8.132	7.987	61 295.5	8g++ [98]
61 313.9	3.0	w	vw	8.174	8.027	61 314.1	9d−+, 9d+− [60, 39]
61 427.5	1.0	m	m	8.473	8.309	61 440.3	9d−− [96]
61 457.0	0.7	s	vvs	8.556	8.388	61 464.0	9d+−, 9d−+ [53, 34]
61 486.5	1.0	s	s	8.641	8.468	61 497.3	9d++ [92]
61 596.6	0.4	w	R	8.984	8.790	61 595.7	9g−− [100]
61 644.3	8.0	vw	w	9.146	8.942	61 646.7	9d−+, 10d+− [51, 29]
61 657.8	0.6	vw	—	9.193	8.986	61 657.3	9g++, 9g+− [70, 22]
61 732.0	2.3	R	m	9.468	9.242	61 741.6	10d−− [95]
61 752.7	8 0	s	w	9.549	9.317	61 762.6	10d−+, 10d+−, 4p5p [42, 26, 16]
61 767.3	5.5	m	m	9.608	9.371	61 774.0	12s−, 10d+−, 4p5p [39, 30, 24]
61 791.5	3.5	m	w	9.707	9.463	61 795.0	10d++ [89]
61 804.2	23	s	m	9.760	9.513	61 811.1	12s−, 4p5p $^3D_2$ [48, 31]
						61 854.9	10g−−, 12s+ [72, 28]
61 862.0	30	w	—	10.015	9.748	61 858.4	12s+, 10g−− [64, 28]
61 915.2	0.7	vs	R	10.267	9.981	61 914.9	10g+−, 10g++ [72, 16]
						61 915.4	10g++, 10g+− [77, 22]
61 919.7	1.5	vs	R	10.290	10.001	61 922.0	11d−+, 11d+− [59, 17]
—	—	—	—			61 961.7	11d−− [97]
61 986.9	1.0	—	vvs	10.640	10.322	61 989.0	11d+−, 11d−+ [65, 22]
62 011.4	2.0	s	s	10.778	10.448	62 016.2	11d++ [89]
62 092.9	0.7	vvs	—	11.275	10.898	62 094.2	12d−+, 11d+− [77, 19]
62 121.2	1.2	w	w	11.464	11.069	62 126.7	12d−− [97]
						62 156.1	14s−, 12d+− [48, 36]
62 156.4	0.9	m	vvs	11.714	11.293	62 157.1	14s−, 12d+− [51, 35]

Table 3. (continued)

E_{exp} (cm^{-1})	Width (cm^{-1})	$^3P_1$	$^3P_2$	$\nu^*_{3/2}$	$\nu^*_{5/2}$	E_{theor} (cm^{-1})	Assignment
62 177.7	1.8	s	s	11.873	11.436	62 181.0	12d++ [89]
62 228.8	0.7	vs	m	12.283	11.801	62230.2	13d−+, 12d+− [78, 16]
62 249.9	1.0	vw	m	12.465	11.962	62 254.0	13d−− [97]
62 286.6	0.6	—	vvs	12.802	12.259	62 287.2	13d+−, 13d−+ [74, 16]
62 305.6	1.6	s	vs	12.988	12.421	62 307.8	13d++ [88]
62 335.9	1.2	vs	m	13.301	12.695	62 337.6	15s+, 14d−+ [60, 30]
						62 335.4°	14d−+, 15s+ [46, 40]
62 350.4	1.0	vw	w	13.460	12.832	62 354.2	14d−− [96]
62 389.8	0.7	w	vvs	13.920	13.229	62 390.0	14d+−, 14d−+ [76, 18]
62 405.4	0.9	vs	vs	14.116	13.397	62 406.4	14d++, 15d−+ [79, 19]
62 421.4	1.1	s	m	14.325	13.576	62 423.0	15d−+, 14d+− [61, 17]
62 432.3	0.9	w	—	14.473	13.702	62 434.8	15d−− [87]
62 450.5	2.8	vw	—	14.732	13.920	62 449.6	17s− [99]
62 472.1	0.6	m	vvs	15.057	14.193	62 471.8	15d+−, 16d−+ [68, 29]
62 483.1	0.6	B	vs	15.231	14.339	62 483.4	15d++, 16d−+ [52, 37]
62 494.1	1.8	vw	—	15.411	14.489	62 495.2	15d++, 16d−+ [43, 28]
62 512.8	2.0	vw	—	15.733	14.755	62 511.8	18s− [94]
62 536.3	0.6	s	—	16.167	15.112	62 536.2	17d−+, 16d+− [63, 37]
62 544.5	0.6	vs	vs	16.327	15.242	62 545.4	16d+−, 16d++ [38, 27]
62 552.0	1.0	—	vw	16.478	15.365	62 553.7	17d−− [84]
						62 558.6	16d++, 16d+− [57, 19]
62 585.8	0.6	vs	w	17.214	15.956	62 586.2	18d−+, 16d+− [81, 13]
62 597.2*	—	R	R	17.485	16.171	62 596.5	18d−−, 17d+− [72, 22]
62 600.5	0.5	m	vs	17.566	16.235	62 601.3	17d+−, 18d−− [47, 27]
62 609.6	1.3	w	w	17.795	16.416	62 610.3	17d++, 17d+− [69, 13]
62 626.4	0.6	s	w	18.243	16.765	62 627.0	19d−+ [78]
62 645.5	0.7	w	s	18.795	17.191	62 646.2	18d+−, 18d++ [73, 16]
62 652.7	0.8	m	m	19.017	17.360	62 653.5	18d++, 20d−+ [63, 30]
62 661.5	1.3	w	vw	19.299	17.573	62 662.0	20d−+, 18d++ [61, 11]
62 684.3	0.8	—	s	20.092	18.166	62 684.2	19d+−, 21d−+ [67, 28]
62 686.3	0.6	m	s	20.166	18.221	62 687.1	21d−+, 19d++ [49, 36]
62 712.4	0.8	B	w	21.218	18.986	62 712.0	22d−+ [70]
62 716.8*	—	R	B	21.412	19.125	62 717.4	22d−−, 20d+− [52, 38]
62 719.4	0.7	w	m	21.530	19.208	62 720.1	22d−−, 20d+− [46, 32]
62 725.5	0.6	R	vw	21.813	19.408	62 725.7	20d++, 22d−+ [62, 19]
						62 733.8°	22s+, 23d−+ [62, 32]
62 734.5	1.0	R	m	22.251	19.715	62 734.8	23d−+, 22s+ [50, 37]
62 739.2	1.0	—	vw	22.491	19.881	62 739.3	23d−− [93]
62 746.5	0.9	w	s	22.879	20.148	62 747.2	21d+−, 21d++ [74, 17]
62 750.2	0.7	s	R	23.084	20.287	62 750.6	24d−+, 21d++ [58, 37]
						62 760.7°	23s+, 26s− [60, 38]
62 761.1	1.5	w	—	23.720	20.715	62 761.2	26s−, 23s+ [62, 38]
62 768.2	1.2	s	R	24.164	21.009	62 768.5	25d−+ [86]
62 771.0*	—	R	R	24.346	21.128	62 771.4	22d+−, 25d−− [56, 25]
62 773.4	0.6	vw	m	24.505	21.232	62 773.9	25d−−, 22d+− [73, 13]
62 777.6	0.8	vw	vw	24.792	21.417	62 777.6	22d++, 25d−+ [55, 19]
						62 783.5°	24s+, 26d−+ [51, 40]
62 784.6	0.9	R	w	25.292	21.738	62 784.2	24s+, 26d−+ [47, 42]
62 787.1	0.6	—	vw	25.479	21.856	62 787.3	26d−− [92]
62 790.2	1.1	vw	—	25.716	22.005	62 790.3	28s− [99]
62 793.0	1.2	m	m	25.935	22.142	62 793.3	23d+−, 23d++ [73, 19]
62 795.1	1.2	m	R	26.104	22.247	62 795.3	27d−+, 23d++ [70, 25]
62 807.6	1.0	R	vw	27.180	22.901	62 807.8	28d−+ [87]
62 811.2*	—	R	R	27.516	23.101	62 810.6	28d−−, 24d+− [76, 19]

Table 3. (continued)

E_{exp} (cm^{-1})	Width (cm^{-1})	$^3P_1$	$^3P_2$	$\nu^*_{3/2}$	$\nu^*_{5/2}$	E_{theor} (cm^{-1})	Assignment
62 812.1	0.8	vw	m	27.601	23.152	62 812.5	24d+−, 24d++ [54, 22]
62 815.4	1.0	w	vw	27.923	23.341	62 815.8	24d++, 28d−+ [47, 37]
62 819.6*	—	R	—	28.349	23.588	62 819.2	29d−+, 24d++ [60, 21]
62 823.2	0.8	w	—	28.731	23.806	62 823.0	31s− [99]
62 826.9*	—	R	R	29.139	24.037	62 827.2	30d−+ [87]
62 828.0	1.5	R	m	29.264	24.107	62 828.4	25d+−, 25d++ [63, 20]
—	—	—	—			62 830.2	30d−− [82]
62 832.6*	—	R	—	29.804	24.406	62 832.6	25d++, 30d−+ [50, 24]
62 836.9*	—	R	—	30.336	24.696	62 836.4	31d−+, 25d++ [71, 9]
						62 837.1°	27s+ [87]
62 838.4	—	sh	—	30.529	24.799	62 838.2	31d−− [91]
62 842.7	1.0	m	m	31.102	25.104	62 843.0	32d−+ [83]
						62 843.1	26d+−, 26d++ [59, 28]
						62 846.8°	34s−, 26d++ [47, 27]
62 847.0*	—	R	—	31.709	25.420	62 847.2	34s−, 26d++ [53, 25]
62 850.8	1.2	R	vw	32.276	25.709	62 850.7	28s+, 33d−+ [68, 24]
						62 856.1	27d+−, 27d++ [65, 26]
62 856.0	1.4	w	m	33.103	26.121	62 856.2	34d−+ [85]
						62 859.4°	36s−, 27d++ [50, 24]
62 859.9*	—	R	—	33.767	26.444	62 859.7	36s−, 27d++ [50, 24]
62 862.5	1.0	w	—	34.233	26.665	62 862.6	35d−+, 29s+ [68, 15]
						62 863.0°	29s+, 37d−+ [82, 13]
62 867.1	2.0	m	m	35.106	27.072	62 867.3	36d−+, 28d++ [85, 10]
						62 867.7	28d+−, 28d++ [69, 19]
—	—	—	—			62 869.2	36d−− [88]
62 870.4*	—	R	—	35.775	27.375	62 870.6	28d++, 36d−+ [45, 30]
62 872.7	—	sh	—	36.265	27.593	62 872.8	37d−+, 28d++ [71, 13]
						62 876.7	38d−+ [86]
62 877.8	1.8	R	m	37.379	28.074	62 877.8	38d−−, 29d+− [50, 38]
						62 878.5	38d−−, 29d+− [47, 34]

It was not possible to observe the '$4p^2$' $^1S_0$ perturber at ~58 535 cm^{-1} through the 3d4p $^3P_1$ intermediate, since both 3d4p $^3P_1$ and $4p^2$ $^1S_0$ are described by almost pure *LS* coupling *and* the $\Delta S=0$ selection rule *holds*. Instead it was observed through the 4s5p $^1P_1$ (Bolovinos *et al* 1992).

Two resonances are ascribed to the excitation of 4p5p levels identified respectively as $^1P_1$ (61 132.1 cm^{-1}) and $^3D_1$ (61 728.9 cm^{-1}). The calculated energies and especially the profiles are in good agreement with the observed ones, as can be seen from table 2 and in the spectra presented later in figures 6 and 8.

Among the three 4p5p $J=2$ levels the lowest one, the $^3D_2$, is calculated to be spread among several levels, but mostly among three of them, with the level at 61 804.2 cm^{-1} containing the larger part of 4p5p $^3D_2$ and thus being identified with it. We have observed all three corresponding resonances and the agreement of their theoretical calculated energies and linewidths is rather good, as can be seen in table 3 and figure 7, presented later. The previous tentative assignment of this $^3D_2$ state (Bolovinos *et al* 1992) is thus proved not to be correct.

These lowest lying perturbers induce localized perturbations of the 3d*nl* series *which are* visible in figures 2 to 4. Additional MQDT calculations, in which the 3d*nl* channels are treated as open channels, permit the determination of the energies of the more

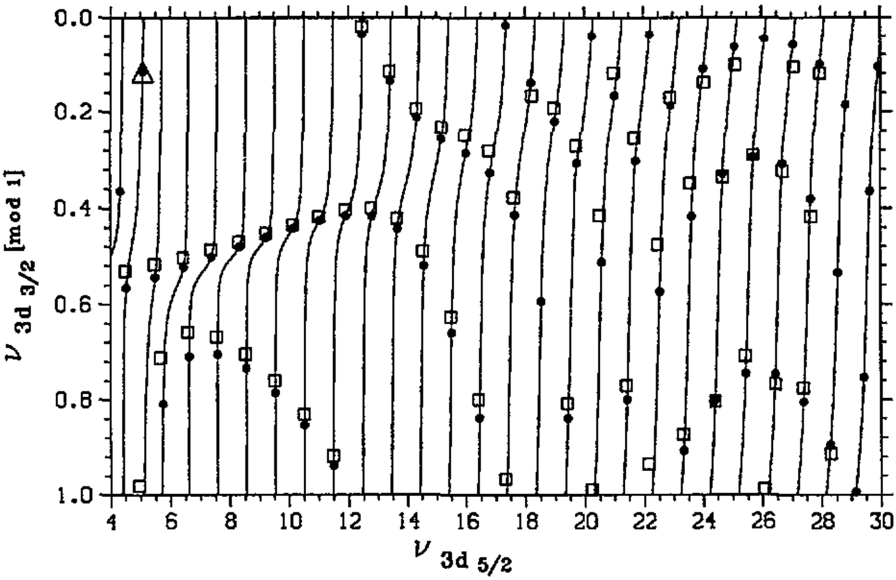

Figure 2. Lu–Fano plot of the $J=0^e$ levels of Ca in the $\nu_{3d_{3/2}}$ (mod. 1) versus $\nu_{3d_{5/2}}$ plane. The curves and theoretical energy levels (●) are calculated with *jj*-coupled effective reaction matrix $K_{\rm eff}^{J=0}$. □, experimental energy levels; △, '$4p^2$' $^1S_0$ level.

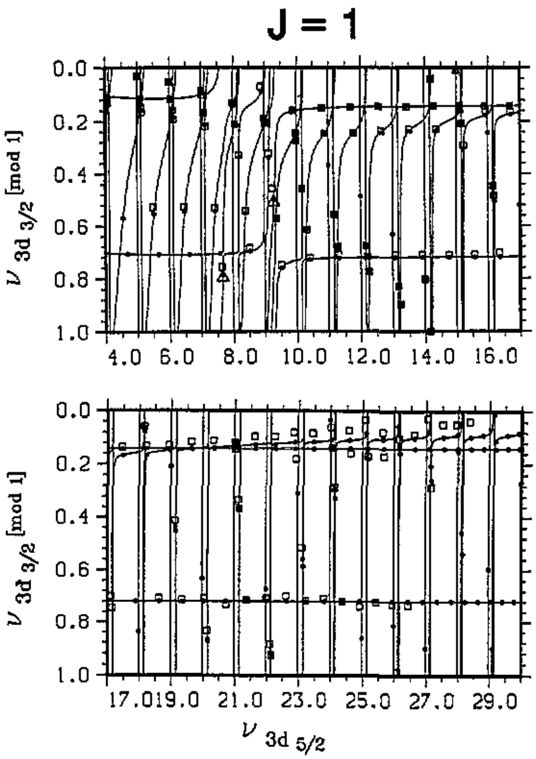

Figure 3. Lu–Fano plot of the $J=1^e$ levels of Ca as in figure 2. The levels with the higher 4p5p contribution are denoted by △.

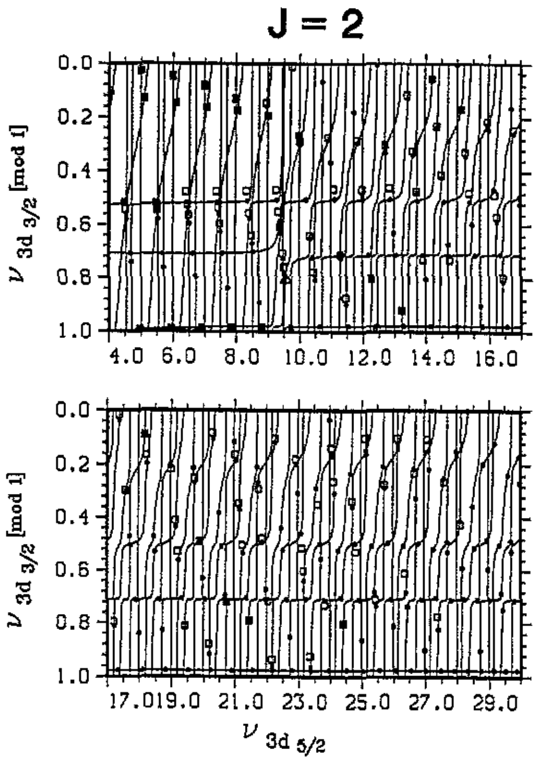

Figure 4. Lu–Fano plot of the $J=2^e$ levels of Ca as in figures 2 and 3.

excited levels of the 4p5p configuration. Thus the $^3P_0$ and $^3P_1$, which are predicted to lie just below the $3d_{3/2}$ threshold, at 62 880 cm^{-1} and 62 910 cm^{-1} respectively, are diluted into the high-lying members of the 3d*n*d $J=0$ and $J=1$ series. The 4p5p $^3P_2$ is predicted to lie at 62 990 cm^{-1} between the two 3d thesholds, while the $^3S_1$ and $^1D_2$ are predicted at 63 360 cm^{-1} and 63 740 cm^{-1} respectively, that is above the $3d_{5/2}$ limit.

5.2. 3dns series

There are three such series, two ($3d_{3/2}ns$ $J=1,2$) converging to the $3d_{3/2}$ limit and one ($3d_{5/2}ns$ $J=2$) converging to the $3d_{5/2}$ one. The theoretical $3d_{3/2}ns$ levels appear as horizontal branches in the Lu–Fano plots of figure 3 and 4 corresponding to nearly constant value for $\nu_{3d_{5/2}}$ (mod 1) $\sim$0.7 (quantum defects $\delta_s \sim 2.3$). The quantum defects for the $3d_{5/2}ns$ levels are also around 2.3. All 3d*n*s $J=1$ levels, except the 3d12s, which is mixed with the nearby 4p5p $^3D_1$ levels, correspond to almost pure $3d_{3/2}ns$ $J=1$ or equivalently 3d*n*s $^3D_1$ levels. In contrast, the $3d_{3/2}ns$ and $3d_{5/2}ns$ $J=2$ series are much more mixed with 3d*n*d levels (see table 3 and the gaps between the branches of the $J=2$ Lu–Fano plot).

The observed 3d*n*s resonances are weak and broad and they are not observed below $n \sim 11$. The $3d_{3/2}ns$ $J=1$ series could be excited for $n=11$ up to $n=36$ (with $n=22$ missing) and through the 3d4p $^3P_0$ and $^3P_1$ intermediates only. As for the two $J=2$ series, less than ten members from each one are seen, half of them through the 3d4p $^3P_1$ intermediate only. The large autoionization widths of these resonances indicate that the 3dns channels are more strongly coupled to the 3sεs and 4sεd coninua than the 3dnd and 3dng ones. Similar behaviour was also found in Sr (Jimoyiannis *et al* 1992, Goutis *et al* 1992).

Because, for a given n, the energy spacing between the $3d_{3/2}ns$ $J=1$ and $J=2$ levels is usually smaller than the widths of the observed resonances, in most cases we cannot resolve these levels. Obviously the $J=1$ are secured if they are seen through the 3d4p $^3P_0$ intermediate, while the $J=2$ states are assigned on the basis of their intensity. For example, for higher n members the $J=1$ levels are calculated to have weak transition probability through the 3d4p $^3P_1$ intermediate, while the $J=2$ have a stronger one. So, whenever such a $3d_{3/2}ns$ state is seen more strongly through the $^3P_1$ and/or is not seen through the $^3P_0$, it is assigned to a $J=2$ value.

As far as the energy difference of the observed $3d_{3/2}ns$ and $3d_{5/2}ns$ levels is concerned it is ~60 cm^{-1}, i.e. equal to the 3d fine structure splitting, for all observed levels with the same n.

5.3.1. 3dnd $J=0$ series. There are two 3dnd $J=0$ series, the $3d_{3/2}nd_{3/2}$ and $3d_{5/2}nd_{5/2}$ ones, which converge to the $3d_{3/2}$ and $3d_{5/2}$ limits respectively. As can be seen from the $J=0$ Lu–Fano plot (figure 2) and the last column of table 1, these two series are strongly mixed in the most part of the observed spectrum. As explained previously (Aymar and Telmini 1991), in the low energy range *LS* labels are more suitable than the *jj*-labels and the 3dnd ^1S series is strongly perturbed by the $4p^2$ ^1S level. For the higher members of the 3dnd series, the *jj*-coupling prevails due to the fine structure of the Ca^+ 3d core. The mixing between the $3d_{3/2}nd_{3/2}$ and $3d_{5/2}$ $nd_{5/2}$ series is indirectly due to the strong mixing between the *LS* coupled 3dnd and 4pnp channels through the electrostatic interaction, which results from the presence of the 4p5p $^3P_0$ level diluted in the high lying 3dnd levels. This indirect coupling of the two 3dnd series is manifested by very irregular variations of both the quantum defect and wavefunction composition for the two series. In spite of these strong mixings, it can be seen in figure 2 that the theoretical values agree well with the experimental data.

With the exception of a couple of cases, excitation of all $3d_{3/2}nd_{3/2}$ levels for $5\leqslant n\leqslant 39$ and $3d_{5/2}nd_{5/2}$ for $5\leqslant n\leqslant 28$ has been observed with a sufficient rate. The theoretical linewidths of the corresponding transitions are in agreement with the experimental observations up to $n\sim 8$. These lowest levels correspond alternatively to narrow and broad resonances; indeed in this energy range the *LS* coupling scheme is well adapted to the description of the resonances. The 3dnd $^1S_0$ levels autoionize thus rapidly towards the 4sεs $^1S_0$ continuum for low n, while for the 3dnd $^3P_0$ ones there is no $^3P_0$ open channel built on the Ca^+ 4s core and the 3dnd $^3P_0$ levels are metastable with respect to the autoionization process. For higher n values the resolution of our method gives larger values than those predicted from the theoretical calculations, where both $^3P_0$ and $^1S_0$ 3dnd ($n>8$) states are calculated to have quite narrow (up to ~0.02 cm^{-1}) widths due to their small coupling with the only available $J=0$ continuum of the singlet 4sεs $^1S_0$ states.

5.3.2. 3dnd $J=1$ series. There are four 3dnd $J=1$ series, the two $3d_{3/2}nd_{3/2,5/2}$ converging to the $3d_{3/2}$ limit and the other two $3d_{5/2}nd_{3/2,5/2}$ to $3d_{5/2}$. As can be seen in the Lu–Fano plot of figure 3, their perturbation by the 4p5p $^1P_1$ and $^3D_1$ levels is rather localized, in contrast to the $J=0$ and $J=2$ series. The regular and relatively simple behaviour of the Lu–Fano plots demonstrates that the 4pp–3dd channel mixing is not very large in the $J=1$ spectrum.

The $3d_{3/2}nd_{3/2}$ series is definitely observed for $6 \leqslant n \leqslant 19$. It has a mostly pure $3d_{3/2}nd_{3/2}$ character except for the $3d_{3/2}10d_{3/2}$ member, which is mixed with some 4p5p $^1P_1$ and $^3D_1$ character. This is consistent with its practically constant quantum defect ($\delta \sim 0.88$ below 4p5p $^1P_1$ and $\delta \sim 0.85$ above 4p5p $^3D_1$) and the negligible avoided crossings of the corresponding Lu–Fano branch in figure 3. The respective transitions are detectable strongly through the 3d4p $^3P_0$ and $^3P_1$ intermediates and show narrow linewidths. Only the perturbed $n = 10$ state has a 10 cm^{-1} width in perfect agreement with the theoretical one.

The $3d_{5/2}nd_{5/2}$ series shows very similar behaviour. We were able to detect the members with $6 \leqslant n \leqslant 17$ and $n = 22$, 23 and 28. For $n \geqslant 11$ they are mostly pure $3d_{5/2}nd_{5/2}$ states while the lowest members have ~80% of such a character due to perturbations by the two 4p5p $^1P_1$ and $^3D_1$ levels (for the $n = 9$ and 10 members at least) and other 3d*n*d series. They correspond to profiles narrower than these associated with $3d_{3/2}nd_{3/2}$ levels, except when the levels are mixed with the 4p5p ones. Their excitation rates for low *n* through all ^3P_J intermediates are strong, while for $n \geqslant 11$ only excitations through the $^3P_0$ and $^3P_1$ are efficient and above $n = 16$ through the $^3P_0$ only.

The $3d_{3/2}nd_{5/2}$ and $3d_{5/2}n'd_{3/2}$ channels on the other hand are strongly mixed among themselves for $n = n' = 6$–10, i.e. in the energy range of the 4p5p $^1P_1$ and $^3D_1$ perturbers, and for $n = 32$–34, $n' = 26$–27, where there are accidental degeneracies between levels belonging to both series. Elsewhere levels are well described in *jj*-coupling. This mixing is evident, too from the large anticrossings of the respective curves in the $J = 1$ Lu–Fano plot, occurring for $\nu_{3d_{5/2}} > 12$, and from the oblique branches in the low energy range ($\nu_{3d_{5/2}} < 12$). This behaviour is typical of the mixing of $nl_{j+}\ l_{j-}$ and $nl_{j-}\ l_{j+}$ *jj*-coupled channels corresponding to the $nll\ ^1L_{J=L}$, $^2L_{J=L}$ *LS* coupled channels, as has been discussed in the case of the 4f*n*f $J = 5$, 6 levels of barium (Luc Koenig and Aymar 1992). In this high energy range, the 4p5p $^3P_1$ perturber is diluted into the $3d_{3/2}nd_{5/2}$ series. This explains the gradual increase of the corresponding quantum defect from 0.75 at $\nu_{3d_{5/2}} \sim 12$ to 0.95 at the $3d_{3/2}$ threshold (see table 2 and figure 3). The effective quantum number of the $3d_{5/2}nd_{3/2}$ series increases from 0.5 to 0.9.

Finally, the $J = 1$ states are, for the most cases, strongly excited through all 3d4p intermediates. Moreover the theoretical energies agree generally well with the experimental ones.

5.3.3. 3dnd J = 2 series. There are four 3d*n*d $J = 2$ series in this case also, two of them converging to the $3d_{3/2}$ and the other two to the $3d_{5/2}$ limit. The $3d_{3/2}nd_j$ series are detected up to $n = 38$ and the $3d_{5/2}nd_J$ up to $n = 28$. The comparison of figures 3 and 4 shows that the 3d*n*d $J = 2$ series are much more mixed than the 3d*n*d $J = 1$.

One series has $\geqslant 95\%$ of $3d_{3/2}nd_{3/2}$ character and a quantum defect $\delta \sim 0.53$ for $n \leqslant 14$ while higher members of the series are mixed with other series and the quantum defects fluctuate between 0.5 and 0.6. The corresponding transitions are weak when the levels are mostly $3d_{3/2}nd_{3/2}$ and rather weak when they are mixed with $3d_{5/2}nd_{3/2}$.

Another series has $\geqslant 85\%$ of $3d_{5/2}nd_{5/2}$ character for $n \leqslant 13$ while higher members are mixed with the $3d_{3/2}nd_{5/2}$ and $3d_{5/2}nd_{3/2}$ series. The quantum defect increases from 0.48 to 0.65 up to $n = 14$ and then fluctuates between 0.5 and 0.65. These levels produce also strong transitions through both 3d4p $^3P_{1,2}$ intermediates.

The levels of $3d_{3/2}nd_{3/2}$ and $3d_{5/2}nd_{5/2}$ series are not perturbed by the 4p5p $^3D_2$ level in agreement with the zero coefficients occurring in the *jj*/*LS* transformation for 3d*n*d levels. On the other hand, since the 3d*n*d $^3P_2$ symmetry corresponds mainly to the $3d_{5/2}nd_{5/2}$ *jj*-coupled levels, the 4p5p $^3P_2$ level, predicted just above the $3d_{3/2}$ limit, is responsible for the scattering of the quantum defects of the higher levels of this series.

Finally the $3d_{3/2}nd_{5/2}$ and $3d_{5/2}nd_{3/2}$ series are strongly mixed among themselves as well as with $3d_{3/2}ns$ for lower n values and with $3d_{3/2}nd_{3/2}$ or $3d_{5/2}nd_{5/2}$ for higher n as we have mentioned already. The $3d_{3/2}nd_{5/2}$, $3d_{5/2}nd_{3/2}$ $J=2$ channel mixing is similar to the corresponding one observed for the $J=1$ channel as discussed above. These levels are seen through both 3d4p $^3P_{1,2}$ intermediates producing strong transitions with similar linewidths as observed in the other 3d*n*d $J=2$ series. These series interact with the 4p5p $^3D_2$ perturber, the largest perturbation occurring for the $3d_{3/2}10d_{5/2}$ level. The members with more $3d_{5/2}nd_{3/2}$ character have a smoothly and fast increasing quantum defect δ from $\sim$0.5 to $\sim$0.85 and up to $n \sim 15$ and then oscillating δ values between 0.8 and 0.9. The quantum defect of the $3d_{3/2}nd_{5/2}$ decreases from 0.87 to 0.6 up to $n=16$ and then oscillates between 0.6 and 0.9.

As *seen* in figure 4 and table 3, several levels show $\sim$1% differences between theoretical and experimental energies with respect to the 3d threshold. However, taking into account the complexity of the spectra, the overall agreement between theory and experiment is satisfying.

5.4. *3dng series*

There is only one 3d*n*g $J=1$ series, the $3d_{5/2}ng_{7/2}$, seen for $n=5$–10, 14–15, which is of practically pure dg character with $\delta \sim 0.01$–0.02, except for the $3d_{5/2}9g_{7/2}$ level close to the 4p5p $^3D_1$ perturber. These levels produce very narrow and weak transitions seen through $^3P_0$ (through the other intermediates they coincide with the stronger transitions populating the 3d*n*g $J=2$ and 3 state).

As far as the $J=2$ series are concerned, there exist three 3d*n*g series: the $3d_{3/2}ng_{7/2}$ and $3d_{5/2}ng_{7/2,9/2}$. The $3d_{3/2}ng_{7/2}$ levels are calculated to be practically pure *jj* coupled; they produce weak and very narrow lines and are seen for $n=5$–9 only (see also the $J=2$ Lu–Fano plot). The $3d_{5/2}ng_{7/2,9/2}$ series produce weak and very narrow lines and they are seen separately for $n=5$–8, while for $n=9$–10 they cannot be resolved with our method. The $J=2$ series are excited through the 3d4p $^3P_1$ intermediate level, while through $^3P_2$ they are masked by the much stronger transitions populating the 3d*n*g $J=3$ states.

Finally the energy difference between $3d_{5/2}ng_{7/2}$ and $3d_{3/2}ng_{7/2}$ is found to be around 60 cm^{-1} for higher n, i.e. equal to the fine structure splitting of the 3d states of Ca^+, which implies that these levels are described well by the *jj* or *jk* coupling schemes.

The 3d4p–3d*n*g transitions are electric dipole forbidden without configuration mixing in either the initial or final levels. Except when accidental degeneracy occurs, the 3d*n*g levels correspond to almost pure (>99%) configurations; therefore excitation of the 3d*n*g levels cannot be ascribed to 3d*n*d–3d*n*g configuration mixing in the final levels. The 3d4p ^3P_J levels have a small (a few per cent) but non-vanishing 3d4f character. On the other hand the 4f–*n*g one-electron dipole matrix elements are an order of magnitude larger than the 4p–*n*d ones, which makes this excitation path the most probable one. We have checked that the MQDT dipole matrix elements connecting the 3d3p ^3P_J levels to the 3d*n*d and 3d*n*g channels are of the same order of magnitude.

5.5. *Absorption profiles*

Theoretical spectra from the different intermediates were computed in the whole energy range investigated experimentally. The theoretical excitation spectrum through a given

3d4p $^3P_{J'}$ is generally obtained by summing different partial cross sections $\sigma_{J'\to J}(E)$; since the calculations do not perfectly describe the relative energy positions between final levels with different J values, it is not always possible to reproduce very satisfactorily total cross sections.

The relative values of the transition intensities are in agreement in most cases with the theoretical predictions. In the cases where a particular state is not detected through a given intermediate, the respective calculated cross section is found to be quite small too. The trends also in the calculated intensities of the different transitions are used to assign observed resonances in cases where our resolution is not sufficient to discern close lying levels, something that happens mostly at high n values.

Figures 5 through 9 show experimental and theoretical spectra for different spectral regions excited through the different intermediate levels. In the experimental spectra lines due to transitions between bound Ca levels are identified by B, while the lines due to 'false' transitions have been omitted, in order to avoid complicating the comparison with the calculated ones. The experimental intensity units are arbitrary, while the theoretical ones are given absolute values in units of Mb.

It is useful though to keep in mind that the experimental intensities depend on the changing laser light intensity profile, as the wavelength λ_2 is scanned (we have tried to make rough corrections to this effect), and on a change in the discharge conditions. On the other hand, because all transitions in a given spectrum start from the same initial state and the final state is always fully autoionized, we do not expect to have any discernible dependence of the (transient) discharge conductivity on the nature of the autoinizing states (autoionization for any final state will produce the same effect on the discharge). The increase of the kinetic energy of the produced electrons, as we excite higher autoionizing states, is not expected either to produce obvious changes to the plasma conductivity, at least within the limited spectral ranges covered in each of the figures shown here. The former of the above mentioned factors, that can affect the OG signal intensity, should make us not fully trust all the relative experimental intensities of the figures shown here, and much more the intensities given in tables 1–3, although their estimation is even more approximate there.

With the above remarks in mind we can see for the majority of our measurements that the agreement between the theoretical and experimental (relative) transition intensities is quite good in general. The agreement is good also for the energy positions and linewidths. However, as already noted, some marked energy differences appear in the energy ranges, where the 4p5p perturbers or some low n levels are involved. Let us look now more closely at each particular spectrum in the figures we have found convenient to present.

Figure 5 shows a spectrum excited through the 3d4p $^3P_0$ and $^3P_1$ intermediate levels and covering a low energy spectral region, where no 4p5p perturbers are present. The agreement in the relative intensities of the lines and their linewidths is very good. As far as the energy positions are concerned, all the $J=1$ lines seem though to be displaced to lower values in the calculated spectrum by $\sim$0.1–0.2% of their term value, while the particular $J=2$ level in this case shows a definitely better (by about a factor of three) agreement.

Figure 6 shows a spectral region, near the 4p5p $^1P_1$ perturber, which is excited through the 3d4p $^3P_1$ intermediate level. Here most levels show increased energy differences (up to $\sim$1% of their term values) and specifically all experimental positions are lower now from the calculated ones. The relative intensities are not that good either. The relative calculated intensities of the transitions to the $3d_{3/2}8d_{3/2}$ $J=2$, $3d_{5/2}8d_{3/2}$

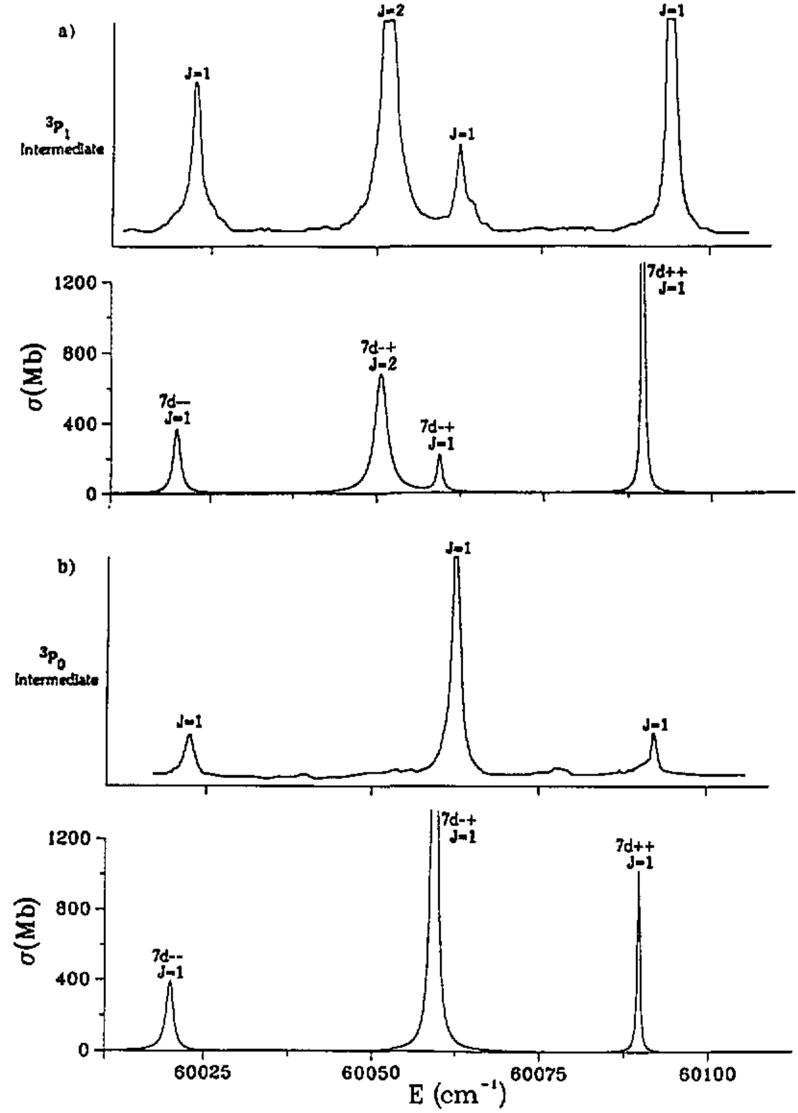

Figure 5. Experimental (top) and theoretical (below) spectra in the energy region of 60 000–60 100 cm^{-1} through (*a*) the $^3P_1$ and (*b*) the $^3P_0$ intermediates.

$J=2$ and $3d_{5/2}8d_{5/2}$ $J=0$ levels are in good agreement with the experimental ones. On the other hand the transitions to the $3d_{3/2}8d_{3/2}$ $J=0$, $3d_{5/2}8d_{3/2}$ $J=1$ and $3d_{5/2}8d_{5/2}$ $J=2$ levels show relatively lower calculated intensities to the previous ones, while the 4p5p $^1P_1$ perturber is calculated to have relatively stronger intensity. In addition the $3d_{3/2}8d_{3/2}$ $J=0$ and $3d_{5/2}8d_{3/2}$ $J=1$ are calculated to have about half their experimental transition linewidths, so their calculated relative cross sections deviate even further, while the transition to the $3d_{5/2}8d_{5/2}$ $J=2$ is calculated to be twice as broad as the experimental one and thus its relative cross section shows a better agreement with the other lines. All other widths are in good agreement. Most probably differences in the fractional contributions of the different configurations that describe any given level,

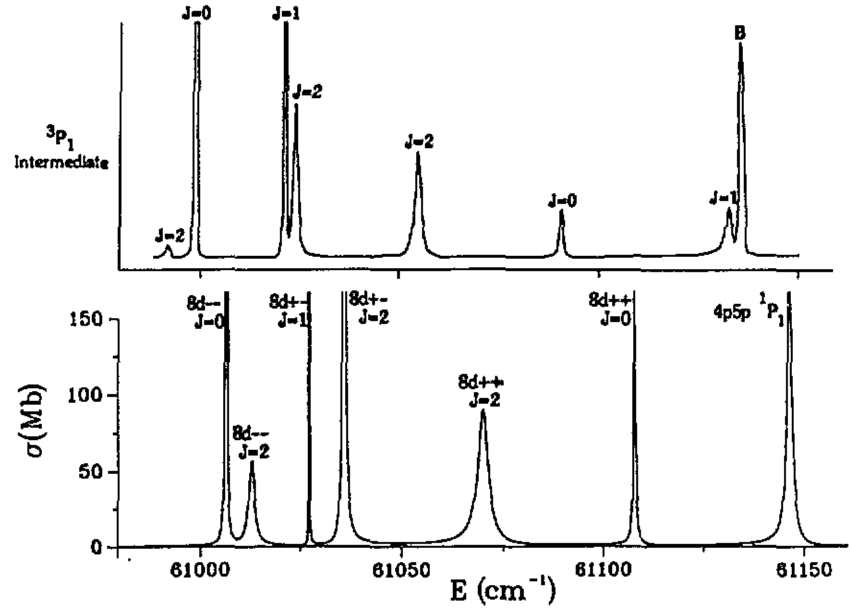

Figure 6. Experimental (top) and theoretical (below) spectra in the energy region of 61 000–61 150 cm^{-1} through the $^3P_1$ intermediate.

may be the reason for the above mentioned deviations. Experimental artifacts do not seem probable to contribute significantly since the trend of the above mentioned deviations is rather irregular.

Figure 7 shows another spectral region, which includes the 4p5p $^3D_2$ perturber that interferes strongly with the nearby $J=2$ levels (see table 3). The linewidths and intensities are quite well reproduced by the calculations for all transitons shown except the broad asymmetrical resonance ascribed to the $3d_{5/2}10d_{5/2}$, where the agreement can be considered quite satisfactory in the spectrum seen through the 3d4p $^3P_2$ intermediate. In the spectrum seen through the 3d4p $^3P_1$ intermediate the peak attributed to the $3d_{5/2}10d_{5/2}$ $J=2$ level is barely seen as a shoulder in the theoretical spectrum. In the same theoretical spectrum the intensity of the very narrow transition to the $3d_{5/2}10d_{5/2}$ $J=0$ level depends strongly on the energy mesh used in the calculation of $\sigma(E)$. On the other hand the energy positions of all $J=2$ lines are calculated to be noticably higher (by ~0.5–0.8% of their term values), while the calculation of the $J=1$ state practically coincides with experiment. A very strong transition beyond 61 825 cm^{-1} is due to a $J=3$ level.

Figure 8 is a spectrum seen through the 3d4p $^3P_0$ intermediate and thus shows only $J=1$ levels, among which the 4p5p $^3D_1$ perturber is included. The intensity and linewidth agreement between experimental and calculated spectral lines is again quite good. However the $3d_{3/2}12s$ line only appears to be a factor of two more intense in the experiment. As far as transition energies are concerned, the 4p5p $^3D_1$ perturber and the $3d_{5/2}10d_{5/2}$ and $3d_{3/2}12s$ levels, which have some 4p5p $^3D_1$ character (see table 2), are displaced to higher energies in the calculated spectrum, while the calculated position of the other line, the $3d_{5/2}10d_{5/2}$, coincides with the experimental one.

Finally figure 9 is another spectrum, seen again through the 3d4p $^3P_0$ intermediate, that covers an energy region for $n \geqslant 11$ away from any 4p5p $J=1$ perturber. The

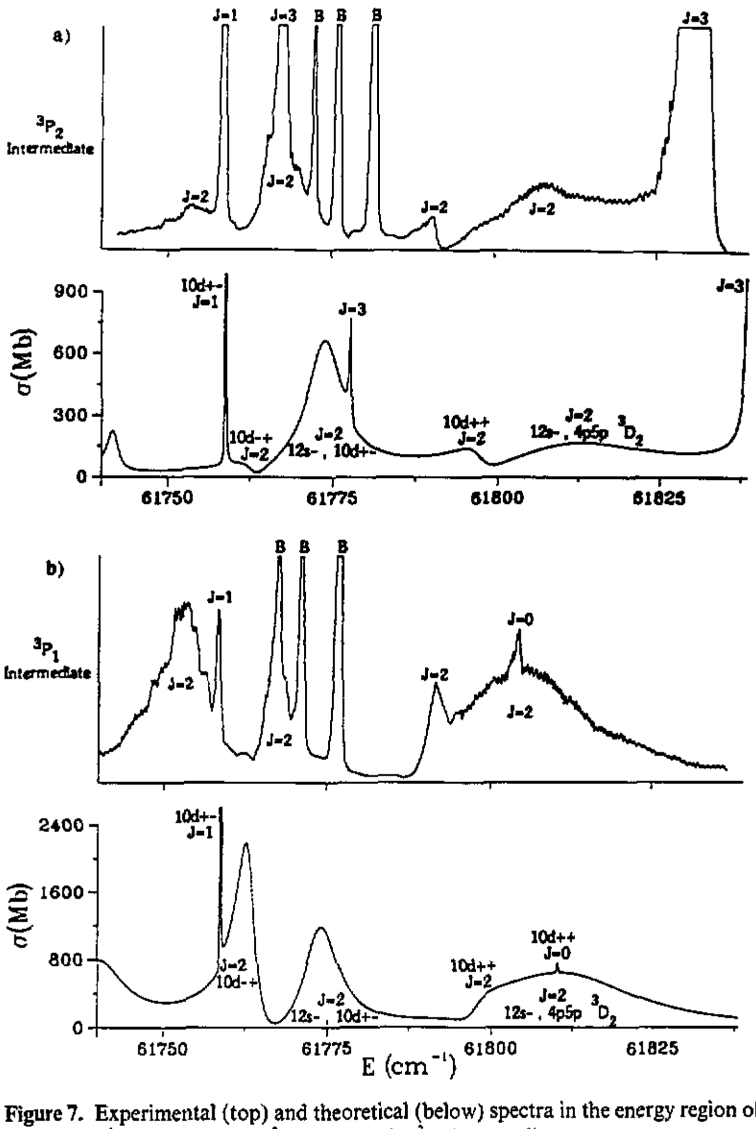

Figure 7. Experimental (top) and theoretical (below) spectra in the energy region of 61 750–61 850 cm^{-1} through (*a*) the $^3P_2$ and (*b*) the $^3P_1$ intermediates.

agreement here is very good in all aspects, line intensities and widths as well as transition energies.

6. Conclusions

Starting from the 3d4s metastable levels of calcium, which are populated by electronic collisions in a DC glow discharge, we used a two-step laser excitation via the 3d4p $^3P_{0,1,2}$ intermediate bound levels to excite about 300 3d*nl* ($l=0, 2, 4$), $J=0^e$–2^e, autoionizing resonances as well as the $4p^2$ or 4p5p perturbers. For the assignment for their total angular momenta, besides using the *J* selection rules for the electric dipole transitions starting from the different intermediate levels, the theoretical predictions were also

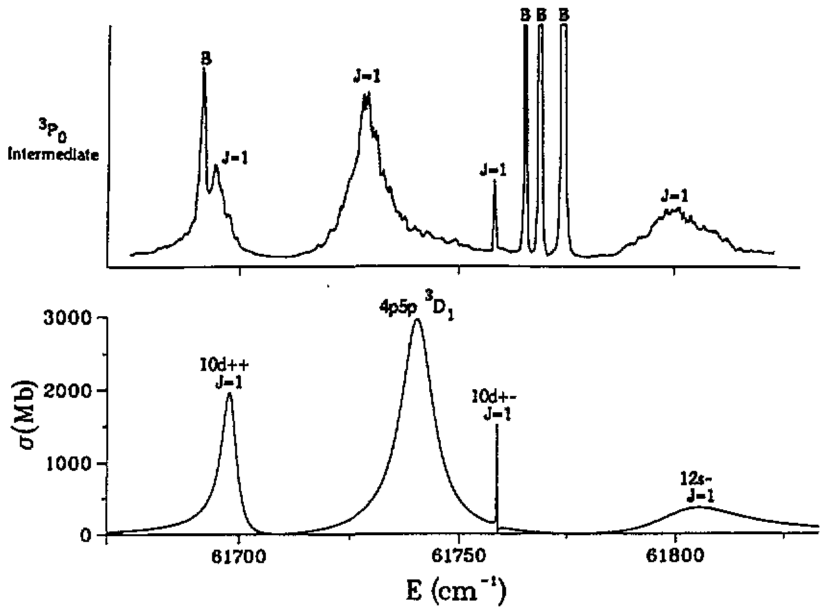

Figure 8. Experimental (top) and theoretical (below) spectra in the energy region of 61 650–61 850 cm^{-1} through the $^3P_0$ intermediate.

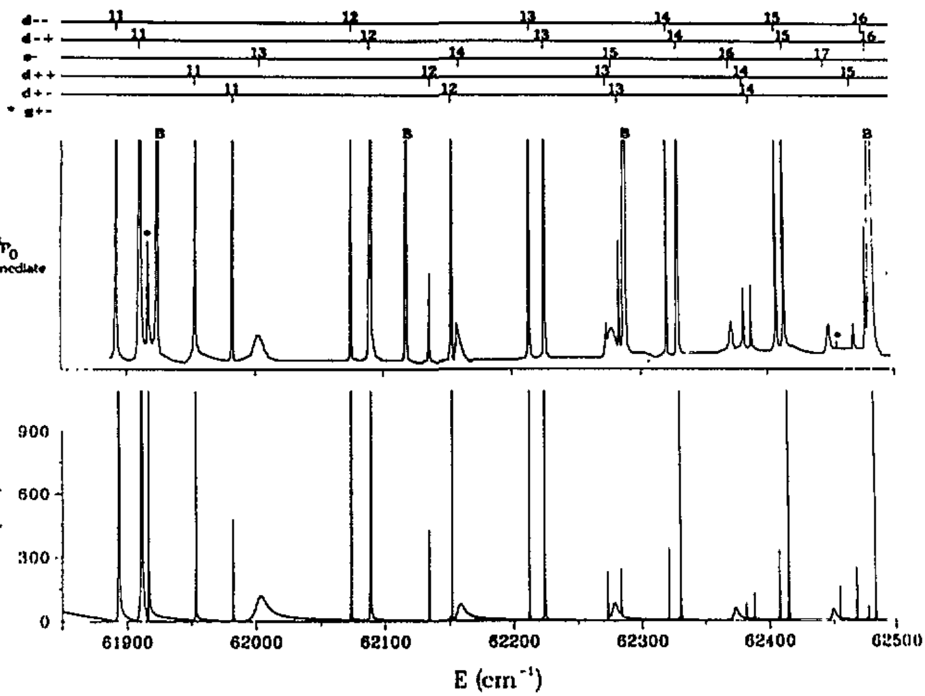

Figure 9. Experiment (top) and theoretical (below) spectra in the energy region of 61 900–62 500 cm^{-1} through the $^3P_0$ intermediate.

indispensable, especially for the identification of the perturbed members of the different series as well as for the assignment of levels that cannot be detected from a particular intermediate, because of low excitation cross sections or overlap with other stronger transitions.

We were able to detect and identify levels belonging to all seventeen $3dnl$ $J=0^e$–2^e series, but for the two $3d_{5/2}ns$ and the four $3d_jng_j$ ones the number of observed members was restricted to no more than ten in each case.

The particular optogalvanic technique used is proved once more to be well suited for the detection of autoionizing Rydberg series up to $n\sim40$. In addition, the availability of several intermediate states for the first step laser excitation makes possible the detection of all existing Rydberg series by choosing the intermediate level which has a high cross section excitation to the particular $3dnl$ levels and their perturbers. The detection of the $4p^2\ {}^1S_0$ perturber through the $4s5p\ {}^1P_0$ and not the $3d4p\ {}^3P_1$ is a characteristic example of this.

From this work we see further that the eigenchannel R-matrix method, coupled to the MQDT formalism, gives a good theoretical description of the observed spectra in spite of their complexity due to several autoionizing Rydberg series interacting among themselves and with low members of $4pnp$ series. In particular the calculated channel mixing between the different $3dnl$ series and with the $4p^2$ and $4p5p$ levels as well as with the $4s\varepsilon l$ continua permits the assignment of all observed levels and produces line intensities and profiles which are in most cases in good agreement with the experimental data. Experimental and theoretical energy positions with respect to the 3d ionization threshold agree generally within 0.1% or less except for lowest lying or perturbed levels. Even for the $J=2$ spectrum the overall agreement is very satisfactory considering the strong channel mixings that give to it a complicated structure.

Finally, although in this work we report the detection of levels with $J=0$–2 only, higher total angular momentum series, up to $J=5$, are expected to be reached easily through other 3d4p intermediates. We are planning to look for them very soon.

References

Aymar M, Luc-Koenig E and Watanabe S 1987 *J. Phys. B: At. Mol. Phys.* **20** 4325
Aymar M and Telmini M 1991 *J. Phys. B: At. Mol. Opt. Phys.* **24** 4935
Bente E A J M and Hogervost W 1989a *J. Phys. B: At. Mol. Opt. Phys.* **22** 2679
—— 1989b *Z. Phys.* D **14** 119
Bolovinos A, Jimoyiannis A, Assimopoulos S and Tsekeris P 1992 *J. Phys. B: At. Mol. Opt. Phys.* **25** L533
Brown C M, Tilford S G and Ginter M L 1973 *J. Opt. Soc. Am.* **63** 1454
Camus P 1974 *J. Phys. B: At. Mol. Phys.* **7** 1154
Camus P, Dieulin M and El Himdy A 1982 *Phys. Rev.* A **26** 379
Camus P, Dieulin M and Morillon C 1979 *J. Physique Lett.* **40** L513
Camus P, Dieulin M, El Himdy A and Aymar M 1983 *Phys. Scr.* **27** 125
Foley M M and Sternheimer R M 1975 *Phys. Lett.* **55A** 276
Garton W R S and Codling K 1965 *Proc. Phys. Soc.* **86** 1067
Goutis S, Aymar M, Kompitsas M and Camus P 1992 *J. Phys. B: At. Mol. Opt. Phys.* **25** 3433
Greene C H and Aymar M 1991 *Phys. Rev.* A **44** 1773
Griffin D C, Andrew K L and Cowan R D 1969 *Phys. Rev.* **177** 62
Jimoyiannis A, Bolovinos A and Tsekeris P 1992 *Z. Phys.* D **22** 577
Jimoyiannis A, Bolovinos A, Tsekeris P and Camus P 1993 *Z. Phys.* D **25** 135
Jones R R, Panming F and Gallagher T F 1991 *Phys. Rev.* A **44** 4265
Kim L and Greene C H 1987 *Phys. Rev.* A **36** 4272
Kompitsas M, Goutis S, Aymar M and Camus P 1991 *J. Phys. B: At. Mol. Opt. Phys.* **24** 1557

Lee C M and Lu K T 1973 *Phys. Rev.* A **8** 1241
Luc-Koenig E 1976 *Phys. Rev.* A **13** 2114
Luc-Koenig E and Aymar M 1992 *J. Physique II* **2** 865
Morita N and Suzuki T 1988 *J. Phys. B: At. Mol. Opt. Phys.* **21** L439
Morita N, Suzuki T and Sato K 1988 *Phys. Rev.* A **38** 551
Nesmeyanov A N 1963 *Vapor Pressure of the Chemical Elements* (New York: Elsevier)
Salih S and Lawler J E 1983 *Phys. Rev.* A **28** 3653
Sternheimer R M 1979 *Phys. Rev.* A **19** 474
Telmini M, Aymar M and Lecomte J-M 1993 *J. Phys. B: At. Mol. Opt. Phys.* **26** 233